MASTER THESIS

Divide and Conquer

Author: Teresa Vaz Martins

Supervisor: Raúl Toral

Universitat de les Illes Balears

Palma de Mallorca, 2010

Abstract

This thesis is about the effects of disorder in the response properties of nonlinear systems subjected to weak forcing. This is a very broad topic that began in the early 80s with the discovery of *stochastic resonance*, a phenomenon by which noise cooperates with a weak forcing to raise it above the threshold for detection. This effect has been observed and described in a plethora of physical and biological systems, that are too many to review here [21; 34]. The typical mechanism involves a bistable system and a matching of time scales that occurs at intermediate levels of noise: the half-period of the forcing, and the residence time inside a potential well, that depends on noise according to Kramer's rate [31].

A parallel line of research was initiated more than 20 years later, in 2006, when it was found [12; 48] that quenched disorder in the form of diversity could play the same role as stochastic disorder as a signal amplifier in extended systems. Most interestingly, it was shown [12; 48] that any source of disorder that fulfils very generic requirements such as leading to symmetric deviations around the average position of the system, should lead to the same resonance effect. When acting upon a bistable system, an intermediate level of disorder doesn't destroy bistability but leads to a lowering of the potential barrier, thereby making a weak forcing suprathreshold. Thus, *disorder induced resonance* provides a theoretical framework that can encompass a wide range of different sources of disorder, including noise in extended systems.

However, there are some types of disorder that do destroy bistability, leading to the appearance of many multistable states separated by

small barriers. This will be the focus of my thesis. In this case, we can also speak of *disorder induced resonance*, since we observe an optimal response for an intermediate level of disorder, and the mechanism is also related to the fact that weak signals become suprathreshold for the small barriers created by disorder. Yet, the situation can only be partially described with the same theoretical tools based on mean field approximations that seem to work in the diversity induced resonance situation [12; 56; 57]. Multistability leads to new behaviors like the possibility to amplify even very weak or very fast signals, with an amplification proportional to the strength of the signal, thus presenting a richer more diverse behaviour in a changing environment.

The outline of this thesis is as follows. Since our aim is to explore the different mechanisms by which different sources of disorder amplify external forcing, we began by comparing in the first Part - Introduction the effects of noise and diversity on a generic bistable continuous system. The second part will be devoted to present the results concerning the effect of competitive interactions in two models: the same bistable continuous model the one addressed in the first Part, and in a discrete opinion formation model.

Contents

I Introduction **1**

1 Stochastic resonance **3**

1.1 The ϕ^4 model 3

2 Diversity induced resonance **8**

2.1 A bistable model 8

2.2 Is diversity required at all? 12

II Resonance induced by competitive interactions **15**

3 The ϕ^4 model **17**

3.1 The bistable model 17

3.2 Signal amplification 18

3.3 Spectral analysis 26

3.4 Conclusions 30

4 Divide and Conquer **33**

4.1 Model of opinion formation 33

4.2 Stochastic and Diversity induced resonance 35

4.3 Repulsive Interactions 36

4.4 Model 37

4.5 Simulation results 39

4.6 Mean-field approach 39

4.7 Mechanism 42

4.7.1 Microscopic point of view 42

4.7.2 Macroscopic point of view 45
4.8 Conclusions 47

5 Conclusions, or what else could be done **57**

A Spectral Analysis **59**
A.0.1 What can the Laplacian represent? 59
A.0.2 Spectral analysis 60

B A method to detect potential wells **64**

C The rewiring algorithm mentioned in the Divide and Conquer chapter **67**

D Publications **69**
D.0.2.1 ϕ^4 model 69
D.0.2.2 Opinion formation model 69

References **74**

List of Figures

1.1 A schematic illustration to explain the mechanism of stochastic resonance. The potential wells represent stable attractors, and the ball, the state of the system. The shape of the potential is perturbed by the weak signal but its bistable characteristics are not destroyed. The periodic signal introduces a bias in the shape of the potential, deepening one of the potential barriers in turn. Source: R. Benzi, Stochastic Resonance: from climate to biology, eprint arXiv:nlin/0702008, 2007. 5

1.2 Results from the simulation of equation (1.3). In upper panel, solution when $A = 0$. In the middle panel the external forcing $Acos(2\pi\omega t)$ while in the lower panel we see the full solution with $A \neq 0$ and noise also different from zero. The small periodic forcing synchronises the random switching from one climate state to the other. Source: R. Benzi, Stochastic Resonance: from climate to biology, eprint arXiv:nlin/0702008, 2007. 6

1.3 The figure shows the Fourier amplitude $|F_X(\nu = \omega)|^2$ for the solution of equation (1.3) for different values of the noise amplitude σ. In the inset we show $|F_X(\nu)|^2$ for $\sigma = \sigma_R$, i.e.the optimal noise for which the Fourier amplitude at $\nu = \omega$ is maximum. Source: R. Benzi, Stochastic Resonance: from climate to biology, eprint arXiv:nlin/0702008, 2007. 7

2.1 The variation of the potential shape as disorder increases. For an intermediate level of disorder, the potential is still bistable, but the wells are closer and the barrier is lower. The optimal level of disorder corresponds to a balance between a desirable low barrier and a not so desirable approximation of the wells. 11
2.2 The resonance peak (lower panel) appears close to an order-disorder transition (upper panel). Source: [48]. 12
2.3 The resonance corresponds to an increase in the amplitude of oscillations (middle panel). Source: [48]. 13

3.1 We plot in a gray scale the stationary probability distribution $P(S)$, in the absence of external signal $A = 0$, coming from numerical simulations of Eqs. (3.1). For better viewing, the distribution has been rescaled by its maximum value at each p. The data show that at $p < p_c \approx 0.44$ the system presents two equivalent absolute maxima for $P(s)$, while there is only one absolute maximum for $p > p_c$. We note, however, that there are many relative maxima for all values of p, specially around the region $p \approx p_c$. Other parameter values are: $N = 200$, $C = 8$. The probability has been computed after averaging over 1000 realisations of the couplings J_{ij} and initial conditions drawn from an uniform distribution in the interval $(-1, 1)$. For the numerical integration we used a fourth-order Runge-Kutta method with a time step $\Delta t = 0.1$. 20
3.2 Spectral amplification factor R versus probability of repulsive links p. Inset: the influence of the amplitude A of the external forcing on the response R. For suprathreshold amplitudes, $A \gtrsim 0.4$, R decreases with A due to the denominator A^2 in the definition of the spectral amplification factor R. $T = 300$, N and C as in Fig. 3.1. 21
3.3 Representative trajectories of the macroscopic variable $S(t)$. Note the large amplitude of the oscillations in the intermediate case $p = 0.44$. The "signal" is the periodic function $A \sin(2\pi t/T)$. Values of N, C and T as in Fig. 3.2, $A = 0.2$. 22

3.4 The influence of the signal period T on the response R. In the inset, we see the response R reaches a constant value for slow enough signals. Values of N, C and A as in Fig. 3.3. 23
3.5 We amplify some representative trajectories (upper panel), and count the number of states through which the system moves in each trajectory (lower panel). Values of T, N and C as in Fig. 3.2. 24
3.6 Coupling-induced resonance. Main plot: the response R shows a maximum as a function of coupling constant C. As shown in the insert, the same maximum appears as a function of the localization measure M, see section 3.3. Values of N, T and A as in figure 3.3 and $K = 0.2$ in the insert. 25
3.7 Coupling-induced resonance, as revealed by the resonant trajectory at optimal $C = 11$. Values of N, A and T as in Fig. 3.3. 25
3.8 System-size induced resonance. Main plot: the response R shows a maximum as a function of the number of units, that follows the same pattern as the maximum M ($K = 0.2$) (inset). Since N decreases the influence of a single neighbor, and C increases it, when the coupling intensity is larger, the optimal system size increases. Values of T and A as in Fig. 3.3. 26
3.9 System size induced resonance, as revealed by the resonant trajectory at optimal $N = 250$. Values of T, A and C as in Fig. 3.3. . . 27
3.10 The participation ratio PR_α is a measure of localization; it estimates the number of eigenvectors components contributing to the Q_α eigenvalue. The eigenvalues at both ends of the spectrum are localized for intermediate levels of disorder. $N = 200$, results after 1000 independent runs. 28
3.11 Measure of localization M: close to the optimal region there is an increase in the fraction of localized open eigenstates. The small dependance of M with K and C is as expected. Parameters: $N = 200$. Inset: $A = 0.2$, $T = 300$. 31

4.1 The coincidence between resonance and order-disorder transtion region. Upper panel: Modulus of the average magnetization as a function of the probability of repulsive links. In the regular networks, the existence of metaestable states reveals itself in a smaller magnetization at $p = 0$. Lower panel: Spectral amplification factor R versus probability of repulsive links p. Parameters are: $a = 0.15$, $\Omega = \frac{2\pi}{100}$, $\kappa = 1$. In the main graph, $N = 100$ and symbols correspond to topologies: ring with $k = 10$ neighbours ($\circ$), square lattice with $k = 8$ neighbours in the Moore neighbourhood ($\square$), and random networks with average number of neighbours $k = 10$ and rewiring probability $q = 0.2$ ($*$) and $q = 1$ ($\triangle$). In the inset, we chose the random network with $q = 1$, $k = 10$, and different curves correspond to sizes $N = 100$ ($\triangle$), 500 ($\triangleleft$), and 1000 ($\triangledown$). . 49

4.2 Evolution of magnetization in time (random network, $q = 1$, $k = 10$). Other parameters are: $N = 100$, $a = 0.15$, $\Omega = \frac{2\pi}{100}$, $\kappa = 1$. . . 50

4.3 Upper panel: Modulus of the average magnetization as a function of the probability of repulsive links according to the mean-field theory for $\kappa = 1$. Lower panel: Spectral amplification factor versus probability of repulsive links according to the mean-field theory for $a = 0.15$, $\Omega = \frac{2\pi}{100}$, $\kappa = 1$. 51

4.4 This image suggests that the step-by-step response we propose is a reasonable mechanism. Their outreach of the perturbations depends on the probability of repulsive links. At the optimal probability $p = 0.26$, the net effect of perturbations accumulates, but after the signal is switched off they don't continue spreading to the whole network. 52

4.5 Spectral amplification factor versus probability of repulsive links for a random network with $q = 1$, $a = 0.15$, $\Omega = \frac{2\pi}{100}$, $\kappa = 1$. Main graph uses $N = 1001$ while the inset shows the case $N = 201$. . . 52

4.6 Spectral amplification factor versus probability of repulsive links for a "no-dispersion" network in which all sites have the same number of positive and negative links. Due to the particular way the network is constructed[41], only values of $p = k/N$ where the total number of neighbours per site, k, is an even integer number are allowed. Parameters are $N = 1001$, $a = 0.15$, $\Omega = \frac{2\pi}{100}$, $\kappa = 1$ (main graph) and $N = 201$ (inset). Note that the amplification region shrinks as k increases. For comparison, we also include as dotted lines the results of figure 4.5. 53

4.7 Comparison between the stable states predicted by mean field and simulations. Upper panel: the effective potential defining the relaxational dynamics according to Eq. 4.17, for different values of the probability of repulsive links p. We considered the case of $k = 100$. Lower panel: Distribution of stable states at the optimal probability $p_c = 0.25$ in the case of an unforced random network with $q = 1$, $N = 100$, $k = 10$, $\kappa = 1$ starting from three different initial conditions: all spins equal to $+1$ (data set indicated as $m(t = 0) = 1$), all spins equal to -1 ($m(t = 0) = -1$) and spins take randomly the value ± 1 ($\langle m(t = 0)\rangle = 0$). 54

4.8 Upper panel: Evolution of the magnetization following a weak signal $a = 0.08$, $\Omega = \frac{2\pi}{100}$, in the case of a random network, $q = 1$, $k = 10$, $\kappa = 1$. The extreme values of the magnetization coincide with the points where the driving value changes sign, they don't take always the same value. This nonstationarity is explained by the influence of the random factors in our model. According to the proposed mechanism, the system walks in multi-steps (Fig. 4.4. The amplitude of the response depends on random factors, such as the sequence of perturbed nodes and their different local fields and connectivities. When the signal is weak and fast, these random factors influence the amplitude of the response, which explains the nonstationarity. Lower panel: Same as figure 4.8 for a slower forcing $\Omega = \frac{2\pi}{333.3}$. If is sufficiently slow, many nodes are perturbed, and at the end the system is able to display the maximum possible response and reach the points $m = \pm 1$. 55

4.9 The influence of annealed disorder. Upper panel: Distribution of stable states at the optimal probability $p_c = 0.26$ in the case of an unforced random network with $q = 1$, $N = 100$, $k = 10$, $\kappa = 1$ starting from random initial conditions ($< m(t = 0) >= 0$). Lower panel: Evolution of the magnetization following a weak signal $a = 0.08$, $\Omega = \frac{2\pi}{100}$, in the case of a random network with annealed disorder in the interaction matrix, $q = 1$, $k = 10$, $\kappa = 1$. 56

C.1 An illustration of the rewiring algorithm. A pair of directed edges A – ¿ B and C – ¿ D is randomly selected. These edges are then rewired in such a way that A becomes connected to D, while C to B, provided that none of these edges already exist in the network, in which case the rewiring step is aborted and a new pair of edges is selected. The rewiring algorithm conserves both the in- and out- connectivity of each individual node. Source: http://www.cmth.bnl.gov/ maslov/ 68

Part I

Introduction

Chapter 1

Stochastic resonance

The phenomenon of *stochastic resonance* was proposed in 1981 to explain the periodicity of ice ages, [45; 47]. It is a somehow counterintuitive effect arising from the cooperation between deterministic dynamics and dynamical disorder or noise. By this effect, a system's coherent response to a weak signal can be optimally amplified by an intermediate level of noise. The prototypical example is that of a continuous variable whose deterministic dynamics is relaxational in a double-well potential. Noise induces jumps between the wells with a rate given by Kramers' expression [31]. The system becomes optimally synchronised with the signal when the signal half-period matches Kramers' rate, as reflected by a maximum value in a suitably defined response. Applications of stochastic resonance were addressed in many areas, and the theory evolved in several directions (see [21; 34] for thorough reviews). In what follows, I will present the main idea of stochastic resonance by illustrating the phenomenon in the climate context where it was originally proposed.

1.1 The ϕ^4 model

The question that led to the discovery of stochastic resonance was: how to explain the periodic recurrence of ice ages? The simplest models of the climate system were energy balance models, that could be described by a bistable dynamics, where the stable states x were either hot or cold.

$$\frac{dx}{dt} = x - x^3 \tag{1.1}$$

Since in reality we observed an alternation of hot and cold periods, the challenge was to find a way to push the climate out of their stable states, and that required an additional ingredient, that should affect the climate with the same periodicity as the occurrence of ice ages. The only known time scale that coincides with that recurrence are the periodic changes in eccentricity of the Earth's orbit around the Sun. Since that perturbation modifies the amount of solar energy received by the Earth, it looked like the ideal candidate to be introduced as a second ingredient in our Eq. 1.1, by means of the addition of a sinusoidal driving.

$$\frac{dx}{dt} = x - x^3 + Asin(\omega t) \tag{1.2}$$

However, the puzzling question is that the so called Milankovitch forcing is not strong enough to induce jumps between the two states of the sytems. In Fig 1.1 we provide a schematic illustration of its modulation effect on the potential. Once the system is perturbed by a small periodic force, it will oscillate within one of the two wells. There would be small climate variations but never something so extreme as a switch from glacial to warm periods.

Should we disregard the coincidence between eccentricity and ice ages recurrence periods altogether, or could there an unknown third factor at play that somehow cooperated with the orbital forcing to induce climate variations? Noise is traditionally introduced to represent the unknown, since noise are fast random variations, whatever their origin. Therefore, we introduce noise in our equation 1.2 and see what happens:

$$\frac{dx}{dt} = x - x^3 + Asin(\omega t) + \sqrt{D}\eta(t) \tag{1.3}$$

where $\eta(t)$ is a gaussian random variable with unit variance ($\langle \eta(t)\eta(t') \rangle = \delta(t - t')$) and D is the noise strength.

If the level of noise is too low, there will be just a few hopping between the two wells, that essentially don't correspond to the regularity observed in the alternation of warm and glacial periods (Fig. 1.2, a). When the noise is too high,

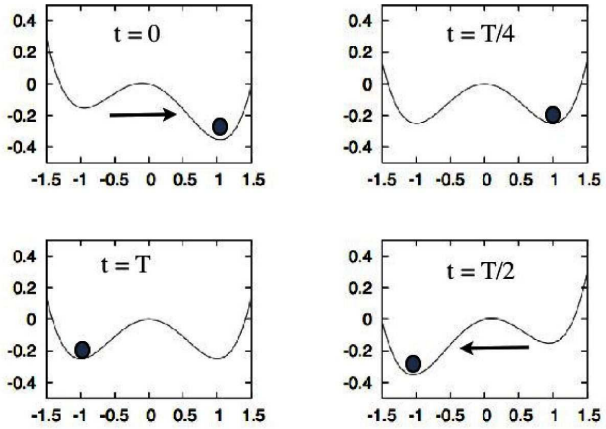

Figure 1.1: A schematic illustration to explain the mechanism of stochastic resonance. The potential wells represent stable attractors, and the ball, the state of the system. The shape of the potential is perturbed by the weak signal but its bistable characteristics are not destroyed. The periodic signal introduces a bias in the shape of the potential, deepening one of the potential barriers in turn. Source: R. Benzi, Stochastic Resonance: from climate to biology, eprint arXiv:nlin/0702008, 2007.

the system behaviour will be completely aleatory, with random hopping between the two states.

The simple yet surprising idea that underlies stochastic resonance is that between these two extremes, there exists a level of noise for which the cooperation between noise and forcing is optimal. This was observed in the numerical experiments of the original works [45; 47], and was finally understood in 1989 [43] as corresponding to a matching between the two time scales involved: the half-period of the forcing, and the mean residence time, that depends on the level of noise according to Kramer's rate [31]. When that happens, the period of oscillations between the climate states matches the period of the signal, as seen in Fig. 1.2, b) and c).

This synchronisation justifies the term resonance, and more specifically *stochastic resonance* since it is induced by tuning the noise intensity. The optimal response appears as a peak in some measure of response at an intermediate amount

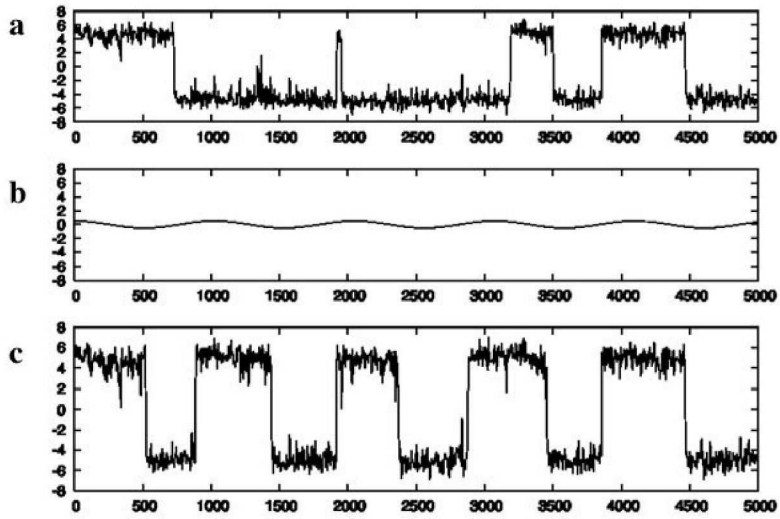

Figure 1.2: Results from the simulation of equation (1.3). In upper panel, solution when $A = 0$. In the middle panel the external forcing $Acos(2\pi\omega t)$ while in the lower panel we see the full solution with $A \neq 0$ and noise also different from zero. The small periodic forcing synchronises the random switching from one climate state to the other. Source: R. Benzi, Stochastic Resonance: from climate to biology, eprint arXiv:nlin/0702008, 2007.

of noise intensity.

A number of measures have been proposed to indicate the optimal response as a function of the noise level, such as the signal-to-noise ratio [6], the residence time distribution [33], information theoretic measures [46; 55], or the spectral power amplification [30].

In our example, a well-suited measure captures the matching between the two time scales that underlies the phenomenon, and can involve the calculation of the Fourier amplitudes at the signal frequency, as it is illustrated in Fig. 1.3.

As it turned out, the climate system could not be described by such a simple model and the stochastic resonance explanation for the appearance of ice ages has to be modified or abandoned altogether [9; 17].

But on the other hand, the concept of stochastic resonance has triggered a

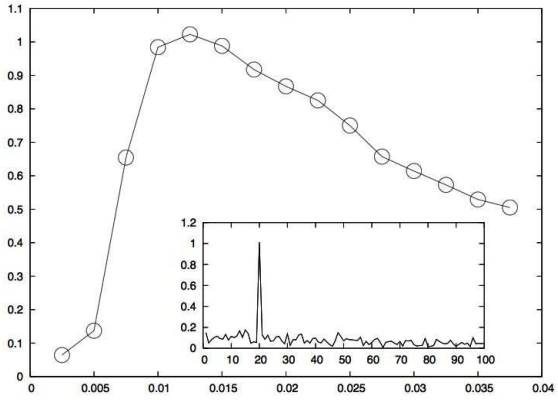

Figure 1.3: The figure shows the Fourier amplitude $|F_X(\nu = \omega)|^2$ for the solution of equation (1.3) for different values of the noise amplitude σ. In the inset we show $|F_X(\nu)|^2$ for $\sigma = \sigma_R$, i.e.the optimal noise for which the Fourier amplitude at $\nu = \omega$ is maximum. Source: R. Benzi, Stochastic Resonance: from climate to biology, eprint arXiv:nlin/0702008, 2007.

wide extension of studies and applications well beyond climate studies, in such diverse areas as lasers [6], SQUIDS [1], or neurons [28], just to mention a few [34], and it has been found to play a role even in systems well beyond the traditional setting of a bistable system subjected to a periodic signal, to include excitable [36] or monostable [29] systems, nonperiodic forcings [26], etc.

Another, more recent, related line of research considers the role that other types of disorder, such as quenched noise (identified with heterogeneity or disorder), can play in producing a resonance effect in systems with many units. Tessone *et al.* [12; 48] have shown that in generic bistable or excitable systems, an intermediate level of diversity in the individual units can enhance the global response to a weak signal. This will be the subject of the next chapter.

Chapter 2

Diversity induced resonance

It was shown in reference [12] that diversity or heterogeneity, in the form of quenched disorder, can play the same constructive role of noise as a signal amplifier. The optimal diversity doesn't preclude the existence of two stable states in the unperturbed system, but changes its position and the height of the potential barrier that separates them. The region of optimal response coincides with a degradation of order, and the optimal response corresponds to an increase in the amplitude of oscillations, and not to a matching between two time scales.

The authors [12] considered two prototypical examples of a bistable and an excitable system, and in what follows we will look into more detail at the bistable example.

2.1 A bistable model

As in the last chapter, we will review the effects of diversity in the response of a forced bistable model.

Instead of a single unit as in Eq. 1.3, let's consider an ensemble of N globally coupled bistable systems, whose dynamics is given by

$$\dot{x_i} = x_i - x_i^3 + a_i + \frac{C}{N}\sum_{j=1}^{N}(x_j - x_i) \tag{2.1}$$

where $x_i(t)$, $i = 1, \ldots, N$ is the position of the i-th unit at time t and C is the coupling strength. Diversity is related to the dispersion in the distribution

of the parameter a_i that controls the relative stability of each individual bistable state. We assume that the a_i's follows a probability distribution function $g(a)$ that satisfies $\langle a \rangle = 0$, $\langle a_i\, a_j \rangle = \delta_{ij}\sigma^2$, where the standard deviation σ measures the diversity.

We will be interested in the macroscopic variable $X(t) = \frac{1}{N}\sum_{i=1}^{N} x_i(t)$, the average position of the units. In the globally coupled case considered here, the coupling amongst units appears only through this macroscopic quantity:

$$\dot{x_i} = CX + (1-C)x_i - x_i^3 + a_i \tag{2.2}$$

Averaging eq.(2.2) over all units, we obtain

$$\dot{X} = X - \frac{1}{N}\sum_i x_i^3 \tag{2.3}$$

As we see, diversity is no longer present in an explicit form in this equation. We recover its influence when we express [14] the position of each unit in terms of a deviation δ_i from the average position as $x_i = X + \delta_i$. Introducing the variance of the deviations $M = \frac{1}{N}\sum_i \delta_i^2$, we relate disorder and diversity when we compute the value of M by averaging over the probability distribution of a_i, as $M(t) = \int da\, g(a)\,[x(t;a) - X(t)]^2$.

If we assume that δ_i are distributed according to an even distribution, or, alternatively, that δ_i is small and we can neglect the third moment, we get, using eq. (2.3), the equation for the macroscopic variable X that describes a bistable system.

$$\dot{X} = X\,(1-3M) - X^3. \tag{2.4}$$

The effective potential is given by

$$V(X) = -\frac{X^2}{2}\,(1-3M) + \frac{X^4}{4}. \tag{2.5}$$

and the equilibrium points are at $X_\pm = \pm\sqrt{1-3M}$.

As M increases, the system goes from bistable to monostable, passing through a region of bistability that is characterised by a lower barrier height and an approximation of the two potential wells, as shown in Fig. 2.1. The influence of

diversity on the response of the system to a weak external signal can already be guessed. If $M = 0$, the units are completely ordered and a weak signal can only induce small oscillations inside a well, as explained in the previous chapter. When disorder is too high, namely for $M > 1/3$, the potential becomes monostable and the response consists of small oscillations within that potential well. By contrast, at an intermediate level of the disorder M the potential is still bistable, but the potential barrier starts to decrease (Fig 2.1, thereby turning the signal supra-threshold. Therefore, an optimal response appears for an intermediate level of diversity, when there is a good trade-off between the two consequences of diversity: the desirable consequence of lowering the barrier, and the not so desirable consequence of approximating the potential wells. For a given signal, the balance is achieved when the barrier is low enough for the signal to become supra-threshold and the potential wells are still sufficiently distant to elicit a big amplitude of oscillations. Fig. 2.2 illustrates the coincidence between the transition order-disorder and an increase in the response of the system that is at the heart of the phenomenon.

The effect translates itself in an increase in the amplitude of oscillations of the macroscopic variable (depicted in bold line in the Fig. 2.3). When there isn't any disorder (upper panel Fig. 2.3) all the units execute small oscillations within a well. When diversity is too high (lower panel in the same figure) the units manifest all types of disorganised behaviour: some remain within one of the wells, while others jump between the two: the end result is that the average position oscillates around zero. It is in the middle panel of Fig. 2.3 that the optimal diversity enables an almost synchronised hoping between the two wells.

Whereas in the case of stochastic resonance in a single unit system the optimal noise is the one for which the rhythm of the system matches the frequency of the signal, here the optimal diversity is the one that amplifies the amplitude of oscillations, because once the stable states are reached, the only source of movement in the system is the external forcing, and any oscillation happens at its rhythm.

Therefore, a convenient measure of resonance evaluates the amplitude of oscillations at the frequency of the signal. As a way of quantifying the coherence of the global response to a periodic forcing $A\sin(2\pi t/T)$, we chose the spectral

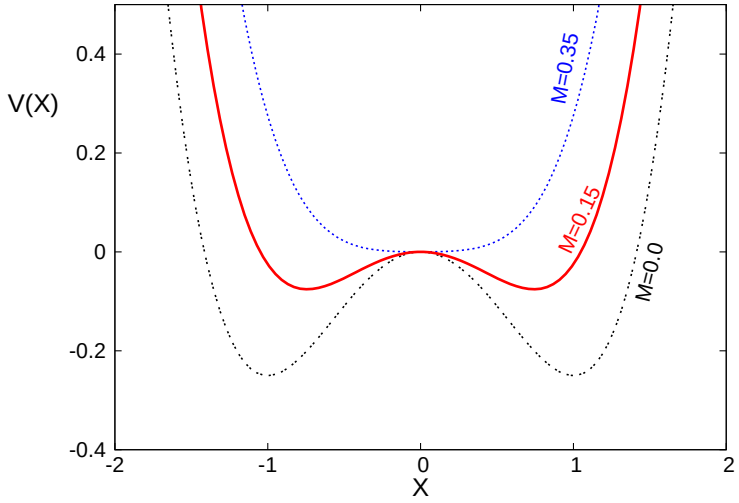

Figure 2.1: The variation of the potential shape as disorder increases. For an intermediate level of disorder, the potential is still bistable, but the wells are closer and the barrier is lower. The optimal level of disorder corresponds to a balance between a desirable low barrier and a not so desirable approximation of the wells.

amplification factor R, defined as the ratio of the output to input power at the corresponding driving frequency Ω [30]:

$$R = 4A^{-2} \left| \langle \mathrm{e}^{-i2\pi t/T} X(t) \rangle \right|^2 \tag{2.6}$$

where $\langle \cdots \rangle$ is a time average, and $X(t)$ is the global response (system's magnetisation): $X(t) = \frac{1}{N} \sum_{i=1}^{N} x_i(t)$.

Large values for R indicate that the global variable $X(t)$ follows the external forcing, while small values of R indicate a small influence of the forcing on the global variable. R is roughly proportional to the amplitude of the oscillations of $X(t)$: if $R < 1$, then the amplitude of the response is less than that of the signal, and vice versa for $R > 1$.

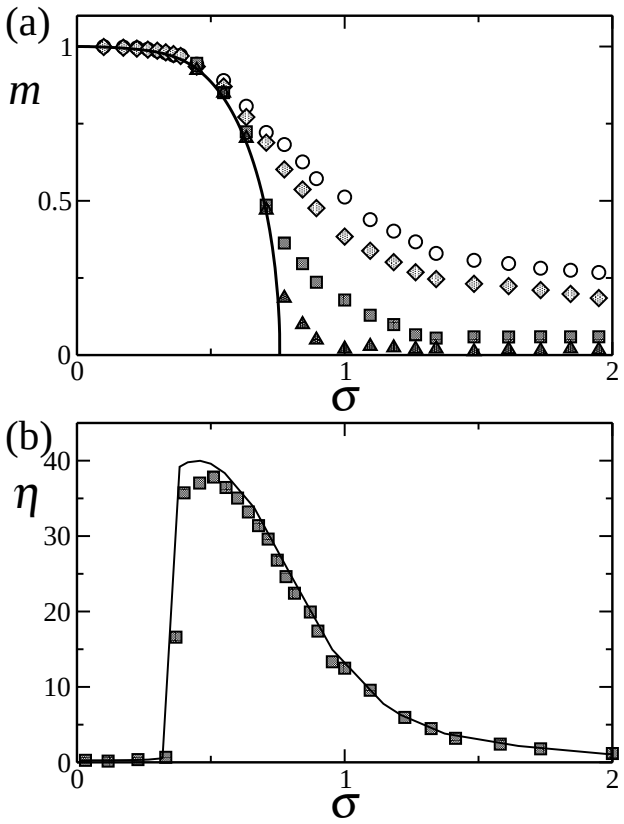

Figure 2.2: The resonance peak (lower panel) appears close to an order-disorder transition (upper panel). Source: [48].

2.2 Is diversity required at all?

This chapter is called *diversity induced resonance*, and the microscopic explanation of the resonance relies on diversity itself, namely, on the assumption that diversity assures that there will always be some units that can respond to the forcing. When the units are identical (and both states are equally stable for all units) the signal is sub-threshold and, because of the coupling, all units remain in the same state. As diversity increases, the signal becomes, for half of its period, supra-threshold for some of the units and forces those units to jump from their less stable state to the other. In the other half of the period, the signal becomes supra-threshold for a different set of units. The units which follow the signal pull

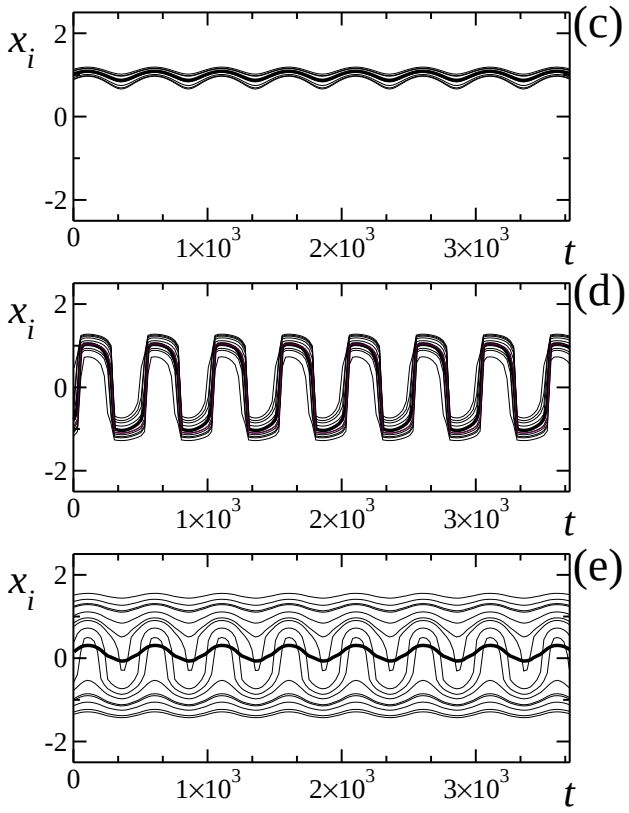

Figure 2.3: The resonance corresponds to an increase in the amplitude of oscillations (middle panel). Source: [48].

the other units, to whom they are attractively coupled, and the collective effect is that a significant fraction of the units is able to respond to the external forcing.

And yet we saw that macroscopically the relevant parameter that optimises the response is the parameter M, that simply measures disorder in the position of the units, whatever its origin. In fact, in the derivation of Eq 2.4 the only assumption was that either the deviations from the mean field are so small that the third moment can be neglected, or, alternatively, that they follow an even distribution. Not only does this make sense in the particular case of an evenly distributed diversity parameter a_i, but it is also applicable to a wide range of situations that don't imply any diversity. In general this loss of entrainment can also be induced by noise (in the case of extended stochastic resonance [25;

61]), competitive interactions, irregular network of connectivity or by some other source.

To better compare the effects of stochastic and diversity induced resonance, we focused here on a ϕ^4 system like we did in the last chapter, but we stress that the same diversity induced resonance effect has been found in different types of systems, such as excitable systems [12], or linear oscillators [49].

Along these lines, the role of the heterogeneous complex network topology in the amplification of external signals has been addressed in [27], and Chen et al. [20] have shown how structural diversity enhances the cellular ability to detect extracellular weak signals. The interplay between noise and diversity in an ensemble of coupled bistable FitzHugh-Nagumo elements subject to weak signal has been considered in [38]. Focusing on the double-well model, Perc *et al.* [39] studied the combined effect of dynamic and static disorder, where static disorder was either diversity, the presence of competitive interactions, or a random field. Namely, they showed that the random presence of repulsive bonds decreases the level of noise warranting the optimal response.

But generic as it is, the assumption of an even distribution or small deviations from the mean field is not universally applicable. It cannot apply, for instance, when we assist to the formation of many metastable states in discrete systems, which can happen when there is frustration due to the presence of repulsive interactions. Does this mean that the disorder induced by competitive interactions is not suitable to get optimal responses, or does it lead to responses with different characteristics? The remainder of the thesis will be devoted to the resolution of this question.

Part II

Resonance induced by competitive interactions

The presence of both repulsive and attractive interactions is not unusual in systems with many units. The existence of inhibitory and excitatory connections in the brain neurons, or a society with friends and enemies are examples of such systems. The emergence of a coherent behaviour in the absence of forcing and in the presence of repulsive links was treated in [23]. There it was shown that one can obtain a more coherent behaviour, in the form of synchronised pulsing, by adding an optimal amount of long-range repulsive couplings in a mixture of excitable and oscillatory units described by the Hodgkin-Huxley model. In the same reference, a similar improvement of the internal coherence in an Ising model with a simple majority-like dynamics in the presence of long-range repulsive links was also shown. Also in [13], an intermediate amount of repulsive links was found to trigger collective firing in an ensemble of active-rotators [52] in the excitable regime.

In this part of the thesis we study periodically forced systems where the only source of disorder is competitive interactions and show that competition in the sign of interactions may also lead to a resonance effect. This resonance can be interpreted as an optimal transmission of the information carried by the external signal, in a kind of "divide and conquer" effect.

Chapter 3

The ϕ^4 model

We will see that competitive interactions can replace noise or diversity in their constructive effect. We focus on the generic globally coupled bistable system, and show that the addition of an intermediate fraction of repulsive links can increase the sensitivity to an external forcing. In particular, we numerically demonstrate that the response of the macroscopic variable to an external signal, is optimal for a particular proportion of repulsive links. Furthermore, we show that a resonance also occurs for other system parameters, like the coupling strength and the number of elements. Resorting to a spectral analysis of the Laplacian [42] matrix, we locate the amplification region, and unveil the mechanism of resonance.

The outline of this chapter is as follows: in section 3.1 we will introduce the model; we show that there is an amplification and discuss how the amplification mechanism is related to a break of stability in section 3.2; and how we can predict the resonance peaks in section 3.3; Conclusions are drawn in section 3.4.

3.1 The bistable model

We consider the same system of N globally-coupled bistable units described by real variables $s_i(t), i = 1, \ldots, N$ under the influence of a periodic forcing.

$$\frac{ds_i}{dt} = s_i - s_i^3 + \frac{C}{N}\sum_{j=1}^{N} J_{ij}(s_j - s_i) + A\sin(2\pi t/T), \tag{3.1}$$

where t is the dimensionless time, C measures the coupling strength amongst the different units and $A\sin(2\pi t/T)$ is a periodic external signal with amplitude A and period T.

The interaction matrix J_{ij} reflects the presence of attractive and repulsive interactions between the units. More specifically, we adopt the following values at random:

$$J_{ij} = J_{ji} = \begin{cases} -1, & \text{with probability } p, \\ 1, & \text{with probability } 1-p. \end{cases} \tag{3.2}$$

The single-element case, $N = 1$, with added noise is the prototypical double-well potential system for which stochastic resonance was first considered. The case without repulsive interactions, $p = 0$, can still be described globally by a bistable potential (see next section) and, in the presence of noise, has been widely studied as a model case for stochastic resonance in extended systems [**?**]; it has also been considered, in the presence of a random field, as a prototypical example for the diversity-induced resonance effect [12]. For $p > 0$, the coexistence of attractive and repulsive interactions is characteristic of a wide class of spin-glass-type systems [15].

We will focus on the macroscopic variable $S(t) = \frac{1}{N}\sum_i s_i(t)$, and use as a measure of response the spectral power amplification factor [30], defined as the ratio of the output to input power at the corresponding driving frequency:

$$R = 4A^{-2}\left|\langle \mathrm{e}^{-i2\pi t/T} S(t)\rangle\right|^2 \tag{3.3}$$

where $\langle\cdots\rangle$ is a time average.

3.2 Signal amplification

It is convenient to analyze first the structure of the steady-state solutions for the system of equations (3.1) in the non-forced case, $A = 0$. The dynamics is relaxational $\dfrac{ds_i}{dt} = -\dfrac{\partial V}{\partial s_i}$ [44], being

$$V(s_1,\ldots,s_N) = \sum_{i=1}^{N}\left[-\frac{s_i^2}{2} + \frac{s_i^4}{4} + \frac{C}{4N}\sum_{j=1}^{N} J_{ij}(s_i - s_j)^2\right] \tag{3.4}$$

the Lyapunov potential. Therefore, the stable steady states are the configurations $(s_1, \ldots, s_N)$ which are absolute minima of V. If there are no repulsive links, $p = 0$, the Lyapunov potential has just two equivalent minima at $s_i = +1$ or $s_i = -1$, $\forall i = 1, \ldots, N$ and, hence, the macroscopic variable will reach the stable asymptotic values $S = +1$ or $S = -1$, depending solely on the initial conditions. Thus we have a typical situation of bistability. As p increases, the absolute minima depart from $S = \pm 1$ and, furthermore, new metastable minima of V appear. The dynamical equations (3.1) may or may not get stuck in one of these minima, depending on initial conditions and the particular realisation of the coupling constants J_{ij}. We have used throughout the paper random initial conditions drawn from a uniform distribution in the $(-1, 1)$ interval, although we have observed the same type of phenomenology when using other random, but still symmetric, distributions such as truncated Gaussian or the Johnson family of distributions.

From our simulations we compute numerically the probability distribution $P(S)$ of the final values of S reached during the dynamical evolution for different realisations of the coupling constants J_{ij} and initial conditions. This is plotted in Fig. 3.1. We can observe a second-order phase transition as the average value $\langle |S(t)| \rangle$ vanishes for $p > p_c \approx 0.44$. One can interpret these results in terms of an effective potential $V_{\text{eff}}(S) \equiv -\ln P(S)$ which has two equivalent absolute minima at $S = \pm S_0(p)$, where $1 > S_0(p) > 0$ for $0 < p < p_c$, and one absolute minimum at $S = 0$ for $p \geq p_c$. The effective potential V_{eff} presents many relative minima for all values of $p > 0$, especially in the critical region $p \approx p_c$, a typical situation for the spin-glass models [15].

We now turn on the forcing $A > 0$ and study the system response, as measured by the spectral power amplification factor R defined above, Eq. (3.3). Consider first the case $p = 0$. For a small, sub-threshold, amplitude A the macroscopic variable $S(t)$ will just execute small oscillations of amplitude proportional to A around the stable values $S = +1$ or $S = -1$. As A increases beyond the threshold value $A_o \approx 0.4$ the amplitude of the forcing is large enough to induce large jumps of the macroscopic variable from $S \approx -1$ to $S \approx +1$ and vice versa. This change of behaviour at A_o appears as a sudden increase in the value of R, as shown in the inset of Fig. 3.2. As the same inset shows, similar behaviour is observed for

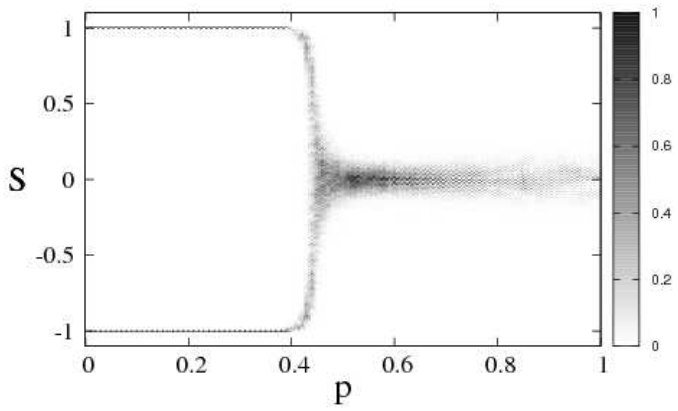

Figure 3.1: We plot in a gray scale the stationary probability distribution $P(S)$, in the absence of external signal $A = 0$, coming from numerical simulations of Eqs. (3.1). For better viewing, the distribution has been rescaled by its maximum value at each p. The data show that at $p < p_c \approx 0.44$ the system presents two equivalent absolute maxima for $P(s)$, while there is only one absolute maximum for $p > p_c$. We note, however, that there are many relative maxima for all values of p, specially around the region $p \approx p_c$. Other parameter values are: $N = 200$, $C = 8$. The probability has been computed after averaging over 1000 realisations of the couplings J_{ij} and initial conditions drawn from an uniform distribution in the interval $(-1, 1)$. For the numerical integration we used a fourth-order Runge-Kutta method with a time step $\Delta t = 0.1$.

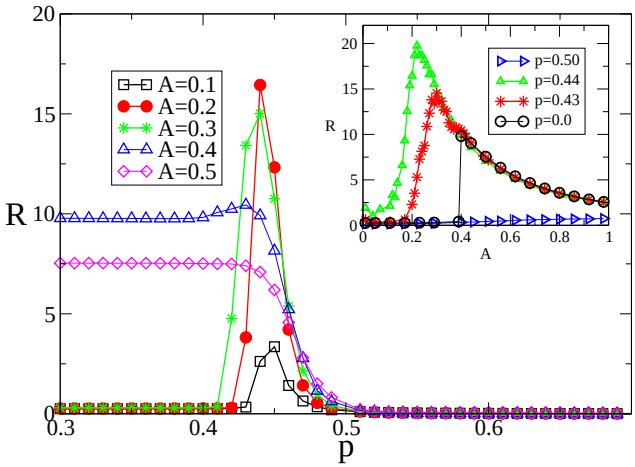

Figure 3.2: Spectral amplification factor R versus probability of repulsive links p. Inset: the influence of the amplitude A of the external forcing on the response R. For suprathreshold amplitudes, $A \gtrsim 0.4$, R decreases with A due to the denominator A^2 in the definition of the spectral amplification factor R. $T = 300$, N and C as in Fig. 3.1.

$0 < p \lesssim p_c$: the response shows a sudden increase for a particular value of the amplitude A and then decreases monotonically. For $p > p_c$, the response is very small and almost independent on the value of A.

More interesting, and the main result, is the dependence of R on the probability p of repulsive links, main plot in Fig. 3.2. We note that there is an optimal probability of repulsive links that is able to amplify signals whose amplitude would be sub-threshold in the case $p = 0$, i.e. $A < A_o$. For suprathreshold signals, $A > A_o$, the presence of repulsive links does no longer lead to enhanced amplification. As shown in the figure, the optimal value for amplification is close to the critical value p_c signaling the transition from bistability to monostability in the non-forced case. The optimal amplification as a function of p can clearly be observed in Fig.(3.3) which shows representative trajectories for $p = 0$ (small oscillations around the value $S = +1$), $p = p_c$ (large oscillations between $S \approx +1$ and $S \approx -1$) and $p = 1$ (small oscillations around $S = 0$).

The existence of an optimal value of the fraction of repulsive p for which signal amplification is maximum is somehow reminiscent of the stochastic resonance

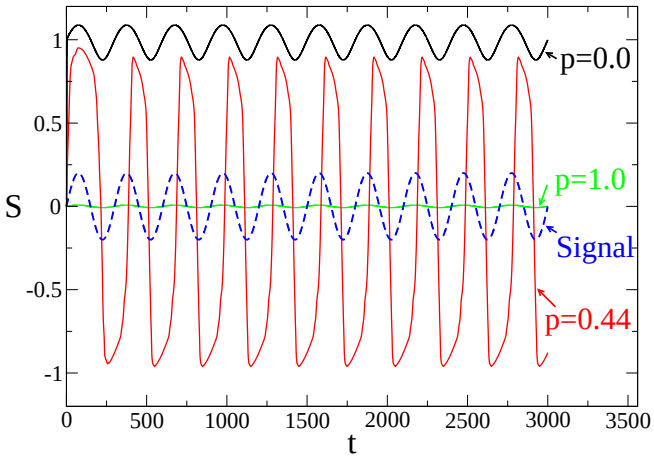

Figure 3.3: Representative trajectories of the macroscopic variable $S(t)$. Note the large amplitude of the oscillations in the intermediate case $p = 0.44$. The "signal" is the periodic function $A\sin(2\pi t/T)$. Values of N, C and T as in Fig. 3.2, $A = 0.2$.

phenomenon. There are some important differences, however. While in stochastic resonance, the response R shows a maximum as a function of period, resulting from the matching between Kramers' rate and the forcing half-period, in our case the same optimal disorder p amplifies responses to signals of every period, as shown in Fig. 3.4. When the signal is slow enough, the system has time to respond to the fuller extent, going to the absolute extrema of the potential, and the amplification factor reaches a constant value, see inset of Fig. 3.4.

It is possible to reinterpret these results in terms of the effective potential $V_{\text{eff}}(S)$ introduced above. The periodic forcing can be seen, approximately, as a periodic modulation to the potential $V_{\text{eff}} - S \cdot A\sin(2\pi t/T)$. As discussed above, the effect of the repulsive links is such that $V_{\text{eff}}(S)$ changes from bistable at $p = 0$ to having many metastable minima at $p \approx p_c$ and a single absolute minimum for $p > p_c$. Hence, the deep potential barrier separating the $S = \pm 1$ solutions for $p = 0$ lowers under the effect of the repulsive links. As a consequence, the modulation induced by the periodic forcing is now large enough, and the global variable is then able to oscillate from the minimum $+S_0(p)$ to $-S_0(p)$ and vice versa. As p approaches p_c a more complicated scenario appears. In this region the

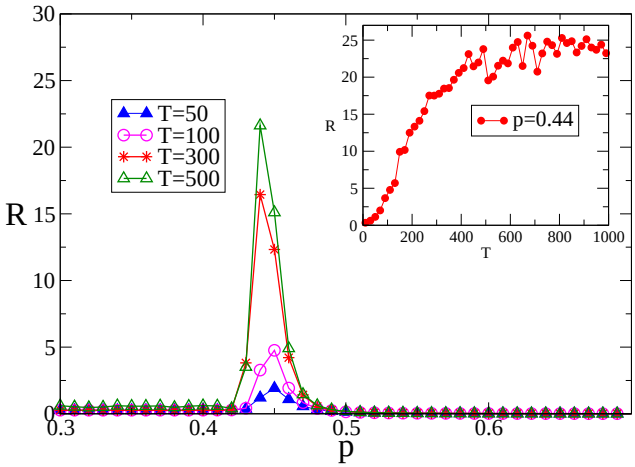

Figure 3.4: The influence of the signal period T on the response R. In the inset, we see the response R reaches a constant value for slow enough signals. Values of N, C and A as in Fig. 3.3.

effective potential presents already a rich structure with many metastable minima in the non-forced case. Those minima can be modified or even disappear by the effect of the periodic modulation. It is particularly illustrative to compare the responses to a suprathreshold signal of amplitude $A = 0.4$ in the case $p = 0$, and to a signal of amplitude $A = 0.2$ (which would be subthreshold in the case $p = 0$) at the optimal fraction of repulsive links $p = p_c$. In both cases, the amplitude of the oscillations is approximately the same, as the system makes large excursions from $S \approx -1$ to $S \approx +1$ and vice versa. However, the shape of the oscillations is rather different, as shown in the upper panel of Fig 3.5. In the $p = 0$ case, the transition from one minimum to the other is rather fast (vertical portion of the dashed line), while in the case $p = p_c$, the transition is slower as the system seems to be spending more time in intermediate states.

To determine what those differences reveal about the underlying effective potential, we have used a method [58] that allows us to detect the number of states a system visits from an analysis of its time series. A typical example is shown in the lower panel of Fig. 3.5. We only detect two states in the global variable S when $p = 0$, corresponding, as expected, to the modulated bistable potential. By contrast, the slight irregularities in the trajectory for $p = 0.44$, hardly visible

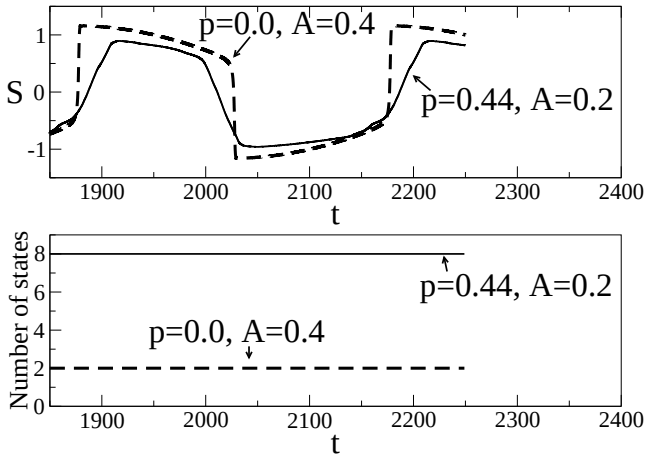

Figure 3.5: We amplify some representative trajectories (upper panel), and count the number of states through which the system moves in each trajectory (lower panel). Values of T, N and C as in Fig. 3.2.

by eye, correspond to several very shallow potential wells. The system evolves through many states at the optimal probability of repulsive links, as shown in the lower panel of Fig 3.5. This image explains why signals of every amplitude and period can be amplified for $p \approx p_c$. In this case, the system can access the many intermediate states, covering a distance proportional to T and A, in case of very fast or very weak signals.

The previous results show that the disorder induced by an intermediate level of repulsive links is an essential ingredient to get an optimal response to the external forcing. This can be explained as, in the absence of forcing, the metastable states correspond to a wide distribution for the values of s_i's. When the forcing is turned on, some units will be responsive to the signal, and then they will pull others which are positively coupled to them. This basic mechanism is further highlighted by the observation of a resonance behaviour with both the coupling constant C and the number of units N.

The resonance with C and some representative trajectories are displayed in Figs. 3.6 and 3.7, respectively. In the weak coupling limit, the units behave basically as independent from each other and, as the signal amplitude A is sub-threshold for a single variable, the overall response is small. In the large coupling

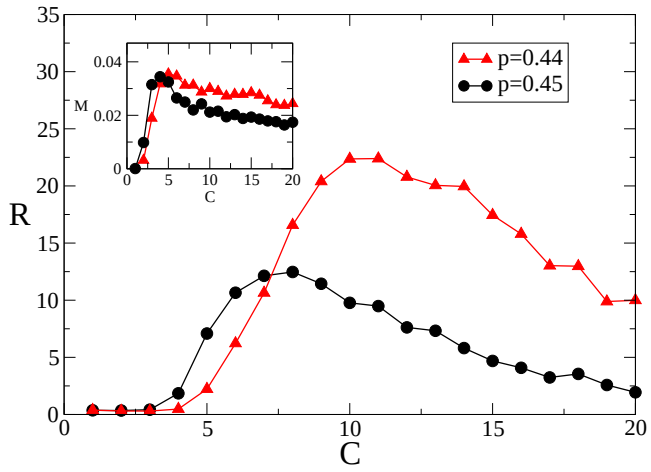

Figure 3.6: Coupling-induced resonance. Main plot: the response R shows a maximum as a function of coupling constant C. As shown in the insert, the same maximum appears as a function of the localization measure M, see section 3.3. Values of N, T and A as in figure 3.3 and $K = 0.2$ in the insert.

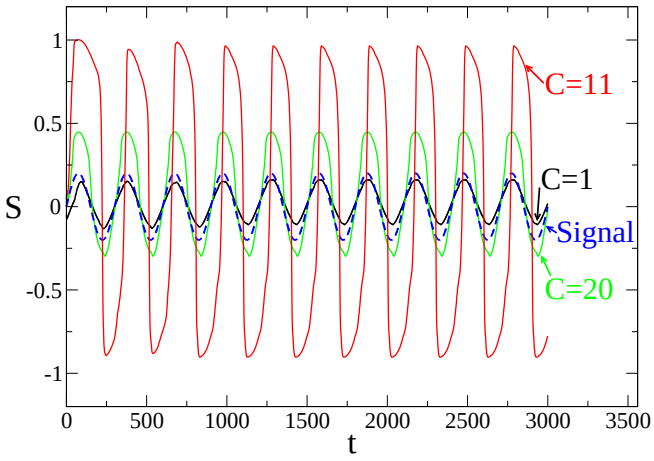

Figure 3.7: Coupling-induced resonance, as revealed by the resonant trajectory at optimal $C = 11$. Values of N, A and T as in Fig. 3.3.

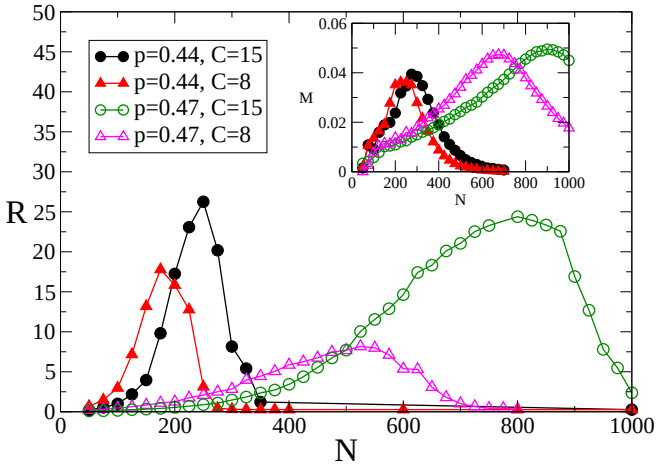

Figure 3.8: System-size induced resonance. Main plot: the response R shows a maximum as a function of the number of units, that follows the same pattern as the maximum M ($K = 0.2$) (inset). Since N decreases the influence of a single neighbor, and C increases it, when the coupling intensity is larger, the optimal system size increases. Values of T and A as in Fig. 3.3.

limit, the interaction term is too big to allow an unit that could first follow the signal to depart from the influence of its neighbors.

The resonance with the number of units N and some representative trajectories is presented in Figs. 3.8 and 3.9. Since fluctuations in the number of repulsive links decrease with N, a larger system requires a greater fraction of repulsive links to achieve the same level of disorder than a smaller system. As a consequence, the response of a larger system is best amplified at a higher probability of repulsive links. As the fraction of repulsive links must not exceed the fraction of positive ones, there can be a limit on how large can a system be, to be able to amplify a signal. The same behaviour, focusing on the number of neighbors was found in a previous study of an Ising-like network model [56].

3.3 Spectral analysis

We have already commented that the optimal probability of repulsive links drives the system to a glassy phase. Anderson [3; 4] has proposed a connection between

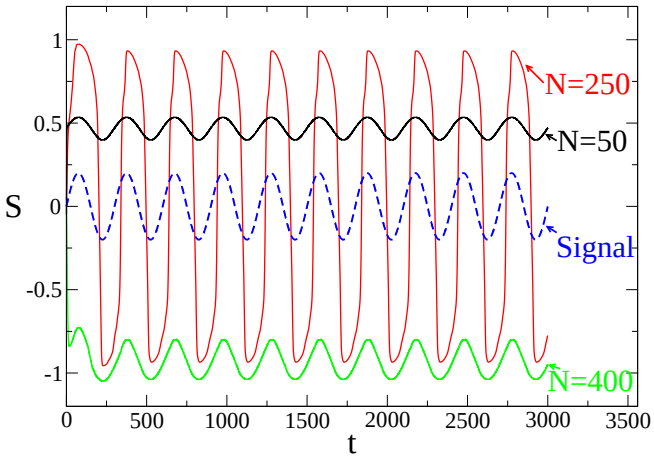

Figure 3.9: System size induced resonance, as revealed by the resonant trajectory at optimal $N = 250$. Values of T, A and C as in Fig. 3.3.

a glass and a delocalization-localization transition, relating the existence of many metastable states with a localization of modes. From this proposal, we retain the idea to work in the eigenspace of the interaction matrix, and to look for the fraction of repulsive links where mode localization becomes significant. This approach has the virtue of not only identifying the steady states, but also to shed light onto how the reaction to perturbations is sustained and spreads along the system, depending on the fraction of repulsive links. In this manner, we hope to locate the region where multistability is expected, and also to understand the mechanism of response to external perturbations.

Following [39], let us define the eigenvalues Q_α and (normalized) eigenvectors $e^\alpha = (e_1^\alpha, \ldots, e_N^\alpha)$ of the Laplacian matrix [42] J'_{ij} :

$$J'_{ij} = J_{ij} - \delta_{ij} \sum_{k=1}^{N} J_{kj}, \tag{3.5}$$

$$\sum_{j=1}^{N} J'_{ij} e_j^\alpha = Q_\alpha e_i^\alpha. \tag{3.6}$$

The effect of the competitive interactions can be described by the so-called participation ratio of eigenvector e^α, defined as $\mathrm{PR}_\alpha = 1/\sum_{i=1}^{N} [e_i^\alpha]^4$. It quantifies the number of components that participate significantly in each eigenvector. A

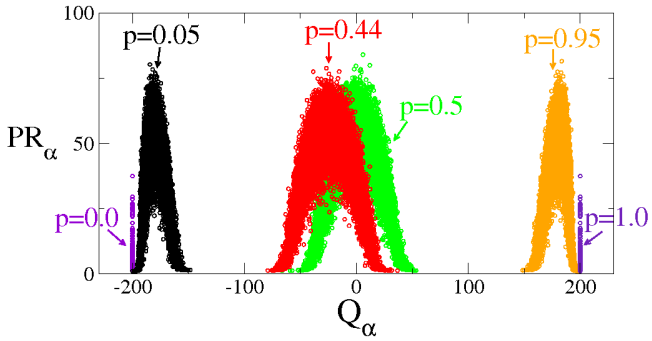

Figure 3.10: The participation ratio PR_α is a measure of localization; it estimates the number of eigenvectors components contributing to the Q_α eigenvalue. The eigenvalues at both ends of the spectrum are localized for intermediate levels of disorder. $N = 200$, results after 1000 independent runs.

state α with equal components has $\mathrm{PR}_\alpha = N$, and one with only one component has $\mathrm{PR}_\alpha = 1$. When $\mathrm{PR}_\alpha = 1$ on a fraction f of elements, and 0 elsewhere, then $\mathrm{PR}_\alpha = f$, which justifies its name. More precisely, we will define "localized" modes as the ones whose participation ratio is less than $0.1N$. Our first observation (Fig. 3.10) is that at the optimal region p there is a significant fraction of positive eigenvalues, and, of those, a significant fraction of the corresponding eigenstates are localized. In this region, we will neglect the coupling between different modes. This approximation allows us to look in more detail at what happens at the optimal region, and in particular at the effect of the coupling strength C and the number N of elements.

Let us focus first on the unforced system ($A = 0$), to see how the presence of the disorder induced by the repulsive links affects a state configuration. We assume each unit i is initially at a given state s_i^o, chosen from a random symmetric distribution and split the variables in the steady state as $s_i = s_i^o + x_i$, being x_i the deviation from the initial condition. We express x_i in the eigenbasis of the J'_{ij} matrix:

$$x_i = \sum_{\alpha=1}^{N} B_\alpha e_i^\alpha, \tag{3.7}$$

Expanding Eq. (3.1) for $A = 0$, multiplying the resulting equation by e_i^α,

summing over all elements i, and approximating averages of the product of initial conditions and eigenvectors by the product of their individual averages (e.g. $\sum_{i=1}^{N} s_i^o e_i^\alpha \approx \sum_{i=1}^{N} s_i^o \sum_{i=1}^{N} e_i^\alpha = 0$), we obtain:

$$\sum_{\beta,\gamma,\eta} F^{\beta\gamma\eta\alpha} B_\beta B_\gamma B_\eta + \left(K - C\frac{Q_\alpha}{N} \right) B_\alpha = 0, \tag{3.8}$$

where

$$F^{\beta\gamma\eta\alpha} = \sum_{i=1}^{N} e_i^\beta e_i^\gamma e_i^\eta e_i^\alpha, \tag{3.9}$$

$$K = \frac{3}{N} \sum_{i=1}^{N} (s_i^o)^2 - 1. \tag{3.10}$$

Neglecting coupling between modes leads to $F^{\beta\gamma\eta\alpha} = 1/\mathrm{PR}_\alpha$ if $\alpha = \beta = \gamma = \eta$ and $F^{\beta\gamma\eta\alpha} = 0$ otherwise. We then obtain the following equation for the amplitude of the α-th mode:

$$B_\alpha^3 + \mathrm{PR}_\alpha \left(K - C\frac{Q_\alpha}{N} \right) B_\alpha = 0. \tag{3.11}$$

According to this approximation, unless $Q_\alpha > \frac{KN}{C}$, the amplitude B_α of the mode α is zero, and any small perturbation vanishes. Otherwise, the mode is said "open" and B_α takes one of the values:

$$B_\alpha = \pm \sqrt{\mathrm{PR}_\alpha \left(C\frac{Q_\alpha}{N} - K \right)}. \tag{3.12}$$

For intermediate amounts of disorder, some open modes begin to appear. The final state of an unit is $s_i = s_i^o + \sum_{\alpha=1}^{N} B_\alpha e_i^\alpha$, and when the initial conditions are random and the open modes α are localized, the system reaches many metastable states, given all the possible combinations of individual states. For this reason, we want to locate a transition to a region with a significant number of localized modes.

To concretize, we define a measure M of localization:

$$M = \frac{N_L^2}{N_O N}, \tag{3.13}$$

where N_O is the number of modes α whose associated eigenvalue Q_α is greater than $\frac{KN}{C}$, and N_L is the number of those modes which, in addition, are localized, i.e. $\mathrm{PR}_\alpha < 0.1N$.

Recalling the definition of K (Eq. (3.10)), we see its value is related to a choice of initial conditions, by the variance of s_i^o. Since we expect multistability to emerge when the initial distribution is more or less uniform, we present results in Fig. 4.17 for values of $K \approx 0$.

At moderate levels of disorder, the localized nodes appear on the tails of the spectra, Fig. 3.10. We confirm that the optimal probability of repulsive links coincides with a maximal localization of open modes in that region, as identified by the peak in M (Fig. 4.17).

In a particular metastable state, the units are randomly distributed, more concentrated near one of the potential wells. Observing the results in Fig. 4.17 for $K \gtrsim 0$, we see that we recover the dependance on C, and that the peak in M still coincides with the optimal probability region. The enhanced responsiveness to an external signal can thus be understood as a consequence of mode localization. Since units can be in different positions, some will be able to answer the signal, and then - since the overall coupling is attractive - pull the others. This is done in an incremental fashion, as confirmed by the localized reaction to perturbations.

The same analysis is valid when we plot M as a function of C or N. We notice a peak in M and accordingly the dependance of the response on C (Fig. 3.6) and N (Fig. 3.8) shows a maximum for intermediate values (insets Fig. 3.6 and Fig. 3.8). When C is small, even if the modes are open, their amplitude B_α is weak, Eq. (3.12). A high fraction of repulsive links, increasing the number of open modes, can overcome this situation to a certain degree, allowing for resonances at a smaller coupling strength.

3.4 Conclusions

In this work, we have analyzed the response to a weak period signal, of a model composed by bistable units coupled through both attractive and repulsive links.

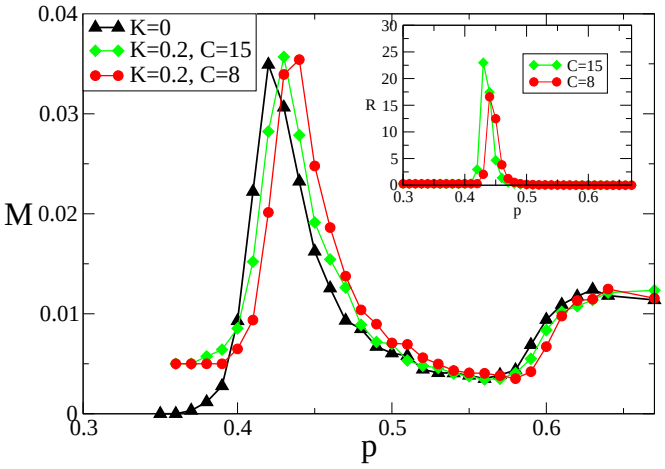

Figure 3.11: Measure of localization M: close to the optimal region there is an increase in the fraction of localized open eigenstates. The small dependance of M with K and C is as expected. Parameters: $N = 200$. Inset: $A = 0.2$, $T = 300$.

Our main result is that the system collective response is enhanced by the presence of an intermediate fraction of repulsive links. Hence, competitive interactions are taken as a source of disorder, as an alternative to previous studies where disorder was induced by noise [34] or diversity [12], and a similar amplification was verified.

We have chosen a very generic double-well model, and have shown that the optimal disorder is the one that destroys the ordered system bistability. The resulting multistable effective potential allows for the amplification of very weak or fast signals. There is not a need to match specific levels of disorder with specific frequencies. Having the optimal disorder, the system becomes more sensitive to external signals of every kind. Furthermore, we have shown that varying the number of elements or the coupling strength in an ensemble of coupled bistable elements can improve the sensitivity to an external forcing. These various ways to increase sensitivity make the phenomenon less dependent on a fine tuning of the proportion of repulsive links, which can be a positive feature in practical applications. Apparently, when the system size becomes very large, it is difficult to get a resonance effect, unless we increase the coupling strength by many times. Arguably, this difficulty can be overcome by other types of network settings [13].

Finally, we have shown that the location of the resonance peaks can be predicted by a spectral analysis of the Laplacian matrix. In heuristic terms [42], the positive eigenvalues of the Laplacian can be seen to express the contribution of the coupling term to the vulnerability of the system to perturbations. We conclude that the location of the amplification region, for a given system size and coupling constant, is reasonably independent of the particular dynamical system. In broad terms, it corresponds to the point where the positive eigenvalues of the Laplacian matrix become localized, signaling a transition to a region where perturbations can accumulate in an incremental manner. The more precise location would depend on the particular dynamical system by means of a condition on open modes.

Competitive interactions are widespread in nature, notably in biological systems. In those systems and others, there has been some studies highlighting their role in achieving a coherent behaviour in the absence of forcing: increasing synchronization [23] or enabling a collective firing [13]. In the present study, we saw they can also help to enhance perception, something that can be potentially relevant in sensory systems.

Chapter 4

Divide and Conquer

We study an Ising model in a network with disorder induced by the presence of both attractive and repulsive links and subjected to a periodic subthreshold signal. By means of numerical simulations and analytical calculations we give evidence that the global response of the system reaches a maximum value for a given fraction of the number of repulsive interactions. The model can represent a network of spin-like neurons with excitatory and inhibitory couplings, or a simple opinion spreading model [23; 32], which is the language we will adopt throughout most of the time in this chapter. In this context, attractive/repulsive links represent friends and enemies. "Divide and Conquer" refers to the fact that in order to force a society to adopt a new point of view, it helps to break its homogeneity by fostering enmities amongst its members.

4.1 Model of opinion formation

In recent years a lot of effort has been devoted to the study of opinion formation models using techniques borrowed from nonlinear and statistical physics [11]. Models can be grouped in two big families, according to whether they consider that the opinion can take a finite set of values , or that it is a continuous real variable [16; 22; 37]. As examples of the models that treat opinions as continuous we can cite the Deffuant [16] and the Hegselmann-Krause [22] models, and as examples of discrete models there is the Sznajd model [54] and several Ising-type variations.

Since we are talking about are opinion formation models, an evolution rule for the opinions has to be provided, which usually implies a definition of whom to interact with, and an interaction rule that at its simplest can take the form of a majority rule that models social pressure.

But in a real society opinion evolution is also affected by external factors, like a political propaganda, advertising, or even a changing biological or economical environment. In many cases a society can only survive as long as it adapts and changes. The influence of mass media has been the focus of several studies [24], some of which addressed specifically the influence of disorder on the efficient spreading of propaganda [7; 32; 57].

A minimalist model of opinion formation, that incorporates the essential ingredients of opinion formation under the presence of an external forcing can represent the possible values of opinions in terms of two options (yes/no), and an interaction rule among neighbours that is a majority rule. Consider a population of N individuals, which, at a given time t, can adopt one of two possible values, $\mu_i = \pm 1$, and evolve according to the following dynamical rule: at time t one of the variables, say μ_i, is chosen at random. The value of this variable is updated according to:

$$\mu_i(t+\tau) = \begin{cases} \text{sign}\left[\sum_j \mu_j(t)\right] & \text{w.p. } 1 - |a\sin(\Omega t)|, \\ \text{sign}\left[\sin(\Omega t))\right] & \text{w.p. } |a\sin(\Omega t)|, \end{cases} \tag{4.1}$$

(w.p. stands for "with probability"). In both cases, if the expression within square brackets is equal to zero, the variable does not change: $\mu_i(t+\tau) = \mu_i(t)$. The first case represents a weighted "majority-rule" in which the opinion of the individual is determined by the sign of average opinion of the other agents j he interacts with. The second case represents the effect of an external forcing of frequency Ω – the intensity $a < 1$ determines the rate at which the signal influences the dynamics of the variable μ_i. The choice of the time step $\tau = 1/N$ defines the unit of time as N updates.

In the global coupling case, the only possible outcome of these rules is an absolute consensus, whose value ± 1 depends on initial conditions. Again we encounter a bistable effective potential, where the depth of the potential well

is related to the number of units that share the corresponding opinion. Unless the probability of interacting with the external signal is very high, there isn't any chance of being able to adjust to environmental changes. Thus the idea to introduce some kind of disorder.

4.2 Stochastic and Diversity induced resonance

Since the depth of the potential well where the population is entrapped is estimated by (half) the number of people that shares our opinion, it seems like a good idea to break consensus a little, by the introduction of some form of disorder. Tessone *et al* [57] changed the interaction rule with the neighbors 4.1 to dilute the social pressure of the neighbors by taking into account individual preferences or biases towards one of the opinions. Their rule becomes [57]:

(i) Select randomly one individual i. Its opinion at time t is modified as :

$$\mu_i(t+dt) = \text{sign}\left[\frac{1}{k_i}\sum_{j\in n(i)}\mu_j(t) + \theta_i\right]. \tag{4.2}$$

The parameter θ_i represents the individual preference and is drawn from a probability distribution $g(\theta)$, which satisfies $\langle\theta_i\rangle = 0$, $\langle\theta_i\,\theta_j\rangle = \delta_{ij}\,\sigma^2$. According to this, the agent i only adopts the average opinion in its neighbourhood $n(i)$ if this average opinion overcomes its preference θ_i.

By resorting to numerical simulations and a mean-field approximation, the authors [57] found that there exists an optimal value of the diversity σ for which the response to a weak forcing takes a maximum value, and that the mechanism is in everything identical to the one described in Chapter 2.

Yet another earlier attempt [32] to aid the propagation of the signal involved the introduction of noise. Kuperman and Zanette [32] used the model 4.1 and included noise as a certain probability to change randomly from one opinion to another. In the context of opinion formation models, noise might represent flicker emotions, free will, or some other external factor [40]. The main point is that now agents can change in a random fashion, not taking into consideration any known factor in the model.

Their aim [32] was to uncover the influence of the newtork topology on the stochastic resonance effect, thus building a bridge between stochastic and disorder induced resonance. Namely, they observed that when the interaction network is regular, the unperturbed system reaches a paramagnetic phase, and that the introduction of some random long range interactions is necessary for the existence of a ferromagnetic state, and as a consequence a bistable situation.

Being interested in stochastic resonance, they turned their attention to this bistable situation enabled by small world networks, finding that as the probability of small world increases, so does the potential depth and as a consequence the strength of the signal needed to invoke a response.

Although they didn't elaborate on it in detail, they hint at the possibility of another type of disorder induced resonance, when mentioning the possibility that very weak forcings could get a response when the population is restricted to local interactions, by the diffusive propagation that could be enabled by the paramagnetic phase. As we will see in the rest of this chapter, this can in fact be achieved by any kind of network as long as we include a mixture of attractive and repulsive links.

4.3 Repulsive Interactions

The homophily hypothesis - the idea that individuals become more alike when they interact - is a basic assumption of the model proposed by Axelrod [5], a mathematician (B.A) that upon turning into a political scientist (PhD) inspired many of present day sociophysics endeavours. Some of the most well-known classical sociological theories [10; 19], on the other hand, have conflict, negotiation or reflexivity at their core and for them order is not equated with a state of absolute consensus, but rather with some form of structure.

The reasons for rejection being the outcome of interaction are many. It can result from a rational discussion, when people realise that even though they share the same opinion, they do it for contradictory reasons, or from the desire to distinguish oneself from some individuals, to define a social status. There has been interest in going beyond the homophily hypothesis to take into account the

possibility of growing apart as a result of interaction, by including *repulsive links* according to some rule [2; 50; 51; 59].

4.4 Model

We consider a set of N spin-like (Ising) dynamical variables $\mu_i(t)$ which, at a given time t, can adopt one of two possible values, $\mu_i = \pm 1$. We will sometimes use the language of a magnetic system, but our aim is quite general and these states can represent, for instance, two different opinions (in favour/against) about a topic, the state of a neuron (firing/not firing), or several other interpretations [23; 32]. The variables are located on the nodes of a given network whose links represent interactions. We assign a weight ω_{ij} to the link connecting nodes i and j and consider only the symmetric case $\omega_{ij} = \omega_{ji}$ (or an undirected network). According to the discussion above, we let the weights take positive or negative values: $\omega_{ij} = 1$ or $\omega_{ij} = -\kappa$ with $\kappa > 0$. The neighbourhood of node i is the set $V(i)$ of nodes j for which a connecting link between nodes i and j exists.

The spin variables evolve according to the following dynamical rule: At time t one of the variables, say μ_i, is chosen at random. The value of this variable is updated according to:

$$\mu_i(t+\tau) = \begin{cases} \operatorname{sign}\left[\sum_{j\in V(i)} \omega_{ij}\mu_j(t)\right] & \text{w.p. } 1 - |a\sin(\Omega t)|, \\ \operatorname{sign}\left[\sin(\Omega t))\right] & \text{w.p. } |a\sin(\Omega t)|, \end{cases} \tag{4.3}$$

(w.p. stands for "with probability"). In both cases, if the expression within square brackets is equal to zero, the variable does not change: $\mu_i(t+\tau) = \mu_i(t)$. The first case represents a weighted "majority-rule" in which the state of the spin is determined by the sign of its *local field* $h_i(t) = \sum_{j\in V(i)} \omega_{ij}\mu_j(t)$. The second case represents the effect of an external forcing of frequency Ω – the intensity $a < 1$ determines the rate at which the signal influences the dynamics of the variable μ_i. The choice of the time step $\tau = 1/N$ defines the unit of time as N updates. We consider both regular lattices (with k neighbours) and random networks of the small-world type. The latter are constructed according to the algorithm proposed by Watts and Strogatz [60]. Denoting by q the rewiring probability (percentage of

short-cuts), the limit $q = 1$ corresponds to a random Erdös/Rényi-type network, $q = 0$ is a regular ring-network and intermediate values of q define a small-world network. We have also considered a square lattice in which a node is linked to the $k = 8$ nodes of its Moore neighbourhood. In each case, links are assigned a strength $-\kappa$ with probability p or a strength 1 with probability $1 - p$. In the case of a random network, the number of links (degree) k_i of node i is a random variable with probability P_{k_i} and average $\langle k_i \rangle = k$. Denoting by k_i^+ and k_i^- respectively the number of positive and negative links of node i, its degree is $k_i = k_i^+ + k_i^-$ and $\langle k_i^+ \rangle = (1-p)k$, $\langle k_i^- \rangle = pk$.

It is worth noticing that, from the formal point of view, the majority-rule is equivalent to a heat-bath stochastic dynamics in the limit of zero temperature[35]. The Hamiltonian is $\mathcal{H} = -\sum_{\langle i,j \rangle} \omega_{ij} \mu_i \mu_j$ (the sum runs over all pairs of neighbours) and the majority-rule always leads to a configuration with less or equal energy. If all the weights ω_{ij} are positive, the ground states are $\mu_i = +1$ or $\mu_i = -1$, $\forall i$, and these ground states are reached independently of the initial condition. If there is a fraction of negative links, the system is of the spin-glass family. The (in general unknown) ground state can have many metastable configurations nearby and the use of the majority-rule may trap the system in one of them.

As a way of quantifying the coherence of the global response to the forcing, we chose the spectral amplification factor R, defined as the ratio of the output to input power at the corresponding driving frequency[30]:

$$R = \left\langle \frac{4}{a^2} \left| \langle\langle \mathtt{m}(t) e^{-i\Omega t} \rangle\rangle \right|^2 \right\rangle, \tag{4.4}$$

where $\langle\langle ... \rangle\rangle$ is a time average, $\mathtt{m}(\mathtt{t})$ is the global response (system's magnetization):

$$\mathtt{m}(t) = \frac{1}{N} \sum_{i=1}^{N} \mu_i(t), \tag{4.5}$$

and $\langle ... \rangle$ is an ensemble average over network realisations, initial conditions and realisations of the dynamics. Large values for R indicate that the global variable $\mathtt{m}(t)$ follows the external forcing, while small values of R indicate a small influence of the forcing on the global variable.

4.5 Simulation results

The main result is that there is a resonance effect, a maximum of the amplification factor R, at an intermediate value of the probability of repulsive links p, as shown in figure 4.1, and that the resonance region coincides with a order-disorder transition. In our case, the degradation of order has its origin in the increasing importance of the inhibitory connections. This is clearly seen in figure 4.1, upper panel, where we plot the standard order parameter m_0 as a function of the probability p of inhibitory links. The optimal probability for resonance p_c (location of the peak of figure 4.1) is found near the phase transition between the ferro and paramagnetic regions.

The existence of this maximum is also visible when looking at the amplitude of the oscillations of the global variable $\mathtt{m}(t)$ – figure 4.2. For small p, $\mathtt{m}(t)$ oscillates with a small amplitude (of order a) around a value close to either $+1$ or -1. As p increases, one clearly notices that the amplitude increases dramatically and $\mathtt{m}(t)$ oscillates around 0. As p increases even further, the amplitude of the oscillations decreases but the global variable still oscillates around 0. This resonance effect appears for all lattices considered, regular or random, for all values of the rewiring probability q.

The existence of this order-disorder transition and its relation to the resonance effects are reproduced by a simple mean-field theory that we develop in some detail in the next section.

4.6 Mean-field approach

At each time step the magnetization $\mathtt{m}(t)$ may change due to the modification of a single variable μ_i. The following relation holds exactly for the ensemble average $m(t) = \langle \mathtt{m}(t) \rangle$:

$$N m(t+\tau) = N m(t) + \langle \mu_i(t+\tau) - \mu_i(t) | \{\mu(t)\} \rangle \tag{4.6}$$

where $\{\mu(t)\} = (\mu_1(t), \ldots, \mu_N(t))$ denotes the particular realization of the μ_i variables and $\langle \ldots | \ldots \rangle$ denotes a conditional ensemble average. By identifying

$\tau = 1/N$ and rearranging we get:

$$\begin{aligned} \frac{m(t+\tau) - m(t)}{\tau} &= \langle \mu_i(t+\tau) - \mu_i(t) | \{\mu(t)\} \rangle = \\ & -m(t) + \langle \mu_i(t+\tau) | \{\mu(t)\} \rangle \end{aligned} \tag{4.7}$$

We now identify the left hand side as the time derivative and use the dynamical rules given by Eq.(4.1) to write:

$$\begin{aligned} \frac{dm(t)}{dt} &= -m(t) + |f(t)| \langle \text{sign}[f(t)] | \{\mu(t)\} \rangle + \\ & (1 - |f(t)|) \left\langle \text{sign} \left[\sum_{j \in V(i)} \omega_{ij} \mu_j(t) \right] \middle| \{\mu(t)\} \right\rangle \end{aligned} \tag{4.8}$$

where we have used the notation $f(t) = a \sin(\Omega t)$. Since the forcing $f(t)$ is independent of the state $\{\mu\}$, then $\langle \text{sign}[f(t)] | \{\mu(t)\} \rangle = \text{sign}[f(t)]$. Moreover $|f(t)| \text{sign}[f(t)] = f(t)$. For the last term of the right hand side of this equation we use the mean-field approximation:

$$\sum_{j \in V(i)} \omega_{ij} \mu_j(t) \approx \left[\sum_{j \in V(i)} \omega_{ij} \right] \cdot m(t) \tag{4.9}$$

where we replace the value $\mu_j(t)$ by the average value $m(t)$.

Now $\sum_{j \in V(i)} \omega_{ij} = k_i^+ - \kappa k_i^- = k_i^+(1+\kappa) - k_i \kappa$, and the mean-field approximation can be rewritten as:

$$\begin{aligned} & \left\langle \text{sign} \left[\sum_{j \in V(i)} \omega_{ij} \mu_j(t) \right] \middle| \{\mu(t)\} \right\rangle = \\ & (-1) \cdot Prob\left(\left[k_i^+(1+\kappa) - k_i \kappa \right] m(t) < 0 \right) + \\ & (+1) \cdot Prob\left(\left[k_i^+(1+\kappa) - k_i \kappa \right] m(t) > 0 \right) \\ & = 1 - 2Prob\left(\left[k_i^+(1+\kappa) - k_i \kappa \right] m(t) < 0 \right) \\ & \equiv G(m(t)) \end{aligned} \tag{4.10}$$

from where we obtain the desired mean-field equation:

$$\frac{dm(t)}{dt} = -m(t) + f(t) + (1 - |f(t)|) G(m(t)) \tag{4.11}$$

The function $G(m)$ can be easily computed in terms of the cumulative probability function F_{k_i} of the binomial distribution of the number of positive links, given that the total number of links is k_i. This is precisely defined as:

$$F_k(x) = \sum_{k^+<x} \binom{k}{k^+} p^{k-k^+}(1-p)^{k^+}. \tag{4.12}$$

In the case $m > 0$,

$$\begin{aligned} &Prob\left(\left[k_i^+(1+\kappa) - k_i\kappa\right] m(t) < 0\right) = \\ &Prob\left(k_i^+ < \frac{k_i\kappa}{1+\kappa}\right) = F_{k_i}\left(\frac{k_i\kappa}{1+\kappa}\right), \end{aligned} \tag{4.13}$$

while, for $m < 0$,

$$\begin{aligned} &Prob\left(\left[k_i^+(1+\kappa) - k_i\kappa\right] m(t) < 0\right) = \\ &Prob\left(k_i^+ > \frac{k_i\kappa}{1+\kappa}\right) = 1 - F_{k_i}\left(\frac{k_i\kappa}{1+\kappa}\right). \end{aligned} \tag{4.14}$$

By averaging over the distribution of the number of neighbours, we get:

$$G(m) = \text{sign}(m) \sum_{k_i} P_{k_i}\left[1 - 2F_{k_i}\left(\frac{k_i\kappa}{1+\kappa}\right)\right] \tag{4.15}$$

P_{k_i} being the probability that a node has k_i links. Within the spirit of the mean-field approximation we assume that all nodes have the same number of links $k_i = k$ and replace the above formula by:

$$G(m) = \text{sign}(m)\left[1 - 2F_k\left(\frac{k\kappa}{1+\kappa}\right)\right]. \tag{4.16}$$

In case of no forcing, $f(t) = 0$, the equilibrium value m_0 of the magnetization satisfies $m_0 = G(m_0)$. A standard analysis of this equation predicts a phase transition separating a regime of non-zero stable solutions $\pm m_0 \neq 0$ from a regime in which the only solution is $m_0 = 0$. The coexistence line is $m_0 = 1 - 2F_k\left(\frac{k\kappa}{1+\kappa}\right)$ and the critical point occurs at $F_k\left(\frac{k\kappa}{1+\kappa}\right) = 1/2$. In figure 4.3 we plot the equilibrium magnetization m_0 as a function of the probability p for fixed k. It is clear from this figure that the mean-field approximation reproduces the loss of order that arises as the proportion p of negative links increases, although the precise location of the transition point is not well reproduced.

In figure 4.3, lower panel, we plot the amplification factor computed after a numerical integration of Eq.(4.11). Qualitatively, the results agree with those of simulations presented in the previous section: there is a resonance effect, i.e. the response shows a maximum as a function of p. The maximum value is reached for a value p_c, close to that signaling the order-disorder transition. Furthermore, it can be noticed that the size of the amplification region, defined as the set of values of p for which $R > 1$, is similar to the size of the transition region, defined roughly as the set of values of p for which the magnetization satisfies $m(p) < 0.5$ and the maximum is achieved at a value of p such that $m(p) \approx 0.2 - 0.3$. As the average number of neighbours k increases, the size Δp of this region decreases as $k^{-1/2}$ and it disappears in the limit $k \to \infty$. Since the relative dispersion in the number of positive links also scales as $\sigma[k^+]/\langle k^+ \rangle \sim k^{-1/2}$, one is tempted to attribute the existence of the resonance to the existence of such a dispersion, a fact already stressed in the study of synchronized oscillations induced by diversity[13]. This is supported by a modified version of the mean-field approach in which the dispersion is strictly equal to 0. This can be achieved by using in (4.16) the probability distribution that would arise if all nodes had the same number k_i^+ of positive links, namely $F_k(x) = 0$ if $x < pk$ and $F_k(x) = 1$ if $x > pk$. As shown in figure 4.3, in this case the amplification region has disappeared altogether.

However, it should be noted that the response in the transition to the amplification region is not continuous in this mean field case. There is a jump at a value p_*, such that $R(p \to p_*^-) = 1$ but $R(p \to p_*^+) > 1$. As discussed later, this discontinuity arises because, in the mean field scenario, the dynamics is governed by a bistable potential. The onset of amplification corresponds to the system being able to jump the potential barrier.

4.7 Mechanism

4.7.1 Microscopic point of view

We now give an explanation of some features of the observed resonance from a microscopic point of view, i.e. analyzing the evolution of individual values of μ_i.

According to the rules (4.3), a chosen node takes the sign of the external signal with a probability $|a\sin(\Omega t)|$, independently of the current system configuration. To enhance resonance, there are two necessary requirements after a node has changed its state: to maintain the perturbation in the next time steps, and to spread it to its neighbours. The crucial issue is then how the local configuration of nodes and links helps (or hinders) this ordering process.

To spread a perturbation, it would be an advantage to have all-attractive couplings; however, to maintain its state, the node cannot be too constrained by its neighbours. With a high homogeneity of the neighbours states and a positive connection with all of them, a perturbed spin would likely be forced to go back to its original state next time it is selected. At the other extreme, when all its connections are negative, a perturbed node is also very much constrained by the state of its neighbours, the local field being maximal for a local anti-ferromagnetic ordering. At an intermediate level of positive and repulsive connections, we have the optimal state. It has a capacity to spread a perturbation to the whole network, but constrains minimally a node that has been perturbed. Due to the combination of attractive and repulsive links, the local field around a node is close to zero. Therefore, if a node changes its state, it possibly won't be forced to return to its previous position after consulting with its neighbours. On the other hand, it is easy to spread a perturbation: if a node had previously a zero local field, after one neighbour has changed, the balance is broken, and it has to align with that neighbour, if the connection is positive.

To illustrate this point we monitored the system's response when the signal is switched on and off, at regular intervals. The goal is to see to what extent perturbations spread after the signal is switched off. These perturbations take the following form: during one unit of time (N updates), taken at regular intervals, the dynamics is such that the randomly chosen nodes adopt the μ=1 state, with probability $A = 0.15$. As shown in Fig. 4.4, those perturbations die out almost immediately for $p \approx 0$ or $p \approx 1$ and only for $p \approx p_c$ are the perturbations able to spread during a finite amount of time.

This microscopic picture will help us to understand some of the observed features. For example, in Fig. 4.5 we show that the amplification region Δp decreases when the number of neigbhors k increases, whereas p_c tends to 0.5.

Both facts agree qualitatively with the predictions of the mean-field theory. It is clear that for large k the condition of a local field close to zero can only be satisfied for a probability of repulsive links near 0.5. This is easily illustrated when one considers the case of p far from 0.5 and a uniform magnetization (at the peak of a signal's cycle). Getting a local field close to zero when the connectivity is high requires many neighbours flips. Since the unit to be updated is chosen randomly at each time step, it is likely that a unit is chosen twice before enough of its neighbours have been perturbed. On the other hand, $p = 0.5$ is the upper limit for the amplification region, because a majority of positive links is necessary to have perturbation spreading. As the proportion of repulsive links approaches 0.5, more neighbours have a negative connection and they will exert, when perturbed, an influence opposite to the signal.

Note that for the resonance to disappear we need formally the limit $k \to \infty$. In a finite network, the maximum value is $k = N - 1$ and, as shown in figure 4.5 for $N = 201$ and $N = 1001$, the resonance does not disappear completely even for the maximum connectivity.

As we did in the mean-field treatment, and in order to isolate the influence of competitive interactions from the disorder induced by the dispersion in the number of links, we also present in figure 4.6 results from random networks when all nodes have exactly the same number of neighbours k and the same proportion p of repulsive links [41]. At variance with the previous results, an almost total reduction of the amplification region can be achieved even for finite values of N, for large enough k. This shows that diversity in the number of positive links is an important ingredient for the robustness of the resonance effect, although that effect doesn't require in general that diversity.

Why does dispersion matter? The precise mechanism is hard to grasp, but it is certainly related to a degradation of order at local level. To decrease the chance of having perturbed neighbours driving several units in the direction opposite to the signal, there have to be many nodes with a clear majority of positive links. But as we saw above – assuming every node had the same number of negative links – those units require many neighbours flips, to maintain their local field close to zero. However, if the nodes are heterogeneous, an unit with a lower than average number of repulsive links can profit from those neighbours that have

many negative connections to other nodes. Since those are more susceptible to changes, their presence decreases the local field, thereby diminishing the need for many neighbours updates. This result confirms the importance of diversity in making the phenomenon more robust, but also shows that we can have an amplification even without diversity.

4.7.2 Macroscopic point of view

In this subsection, we consider the explanation of the resonance from the macroscopic point of view, i.e. we look at the behaviour of the collective variable (magnetization) $m(t)$. We assume that the dynamics of this macroscopic variable in the no-forcing case, $f = 0$, can be described in terms of relaxation in a potential function $V(m)$. The absolute minima $\pm m_0$ of the potential give the rest states which are separated by a potential barrier ΔV. This picture has proved to be valid in other problems with diversity in the parameters [12] and it certainly holds in the mean-field limit where, according to the previous section, the dynamical equation is $\frac{dm}{dt} = -\frac{dV}{dm}$ with a potential given by:

$$V(m) = \frac{m^2}{2} - M(p)|m| \tag{4.17}$$

with $M(p) = 1 - 2F_k\left(\frac{k\kappa}{1+\kappa}\right)$ running from $M(0) = 1$ to $M(1) = -1$. Fig. 4.7, upper panel, illustrates the effect of repulsive links on the shape of the potential, according to the mean field predictions. There are two minima of the potential, $m_0 = \pm M(p)$ for $M(p) > 0$, and a single minimum $m_0 = 0$ for $M(p) < 0$, or $p > p_c$, the critical point. For small p the barrier separating the two minima is high and it can not be overcome by the effect of the weak forcing $f(t)$. The only effect of the forcing is a small oscillation around one of the minima (chosen by the initial conditions). As p increases, the two minima of the potential get closer to each other and the barrier separating them decreases such that, at a particular value of p the forcing is able to overcome the barrier and $m(t)$ oscillates between the two minima $\pm m_0$. As p crosses the critical value p_c, the two minima merge at $m_0 = 0$, the barrier disappears and the effect of the forcing is reduced again to small oscillations around a single minimum.

To apply this potential image beyond the mean-field approximation we need to include an important modification. As discussed before, the energy landscape is that of a spin-glass with many metastable states and two absolute minima $\pm m_0$. As a consequence, in the no-forcing case, the final state reached depends strongly on initial conditions. This is illustrated in figure 4.7, lower panel, where we plot the probability distribution of the final magnetization. If the initial state is the ordered state $\mu_i = +1$ (resp. -1) $\forall i$, the final magnetization is peaked near $\mathtt{m} = \mathtt{1}$ (resp. -1). If the initial state adopts $\mu_i = \pm 1$ randomly, then the final magnetization is peaked around $\mathtt{m} = \mathtt{0}$. This reflects the existence of many barriers separating the metastable states from the absolute minima of the potential. When the forcing is introduced, it has to be able to overcome all these intermediate barriers. The final image is that of a particle moving in a "rugged" potential. As p increases, the height of those barriers decreases and the forcing is able to explore a larger fraction of the configuration space, but not necessarily leading to trajectories ending in the absolute minima of the potential. This can be seen in figure 4.8 where we show the effect of a forcing weaker than that used in figure 4.2. The magnetization oscillates around a mean value that drifts with time. If we enlarge the period of the forcing – Fig. 4.8, lower panel – the oscillations become wider and the system has now enough time to reach the equilibrium minima close to $m_0 = \pm 1$.

The origin of the discrepancy in the results of simulations and mean field lies in the approximation 4.9. When we consider a annealed version, where disorder is not correlated in time, we can recover a bistable potential as it is predicted by the mean field. In the annealed version, the neighbourhood is fixed but the relationship matrix $w_{ij}$is redefined randomly at each time step. In fact, this version could be more accurate to represent, for instance, plasticity in the brain, or a society without personal prejudices: here people are not always opposed to the position of the same neighbors. Another option is to allow for a transient time, when the connectivity changes randomly, and then freeze the connections. This transient time with annealed disorder is a way of averaging over the distributions of repulsive links, thereby making the system less dependent on initial conditions. This scenario might model a society where a diffusive animosity finally crystallises into entrenched positions of friends and enemies, or in another context, the known

fact that brain plasticity is higher in initial stages. Even though the microscopic mechanism of resonance is the same in all the three scenarios, the macroscopic picture is somewhat different. In the temporarily annealed scenario, the bimodal distribution of stable states in Fig. 4.9 suggests a bistable nonlinear dynamics. We don't show here the annealed disorder case, because it looks similar to Fig. 4.9 . However, there is a difference: in the annealed disorder scenario the system oscillates randomly between the potentials wells, whereas in the temporarily annealed case, usually (not always...) a stable state is reached when the population is not being forced by an external signal. Comparing the lower panel of Fig. 4.9 with the upper panel of Fig. 4.8 we observe that the response to very weak fast signals is much more pronouced when the relationship matrix changes with time.

Just like the introduction of diversity in the number of repulsive links made the response more robust against changes in the number of elements, so does the introduction of some kind of stochastic disorder makes the system more sensitive to weaker signals.

4.8 Conclusions

We have used Monte Carlo simulations and analytical (mean field) calculations to investigate the response of a system of two-state units, with both attractive and repulsive interactions and majority-rule dynamics, to a weak periodic signal. For both regular and random networks, we have found that competing interactions can enhance the system response – a kind of "divide and conquer" strategy. In each case, a resonance was found for an optimal percentage of negative links which depends on the model parameters. Applications include opinion dynamics and neuron networks but the model is generic enough to predict that the same type of effect can be found in other systems. We have carried out a detailed analysis for an opinion model first introduced by Zanette and Kuperman[32] but we want to stress that the "microscopic" details of the model are not essential for the resonance phenomenon. In fact, we have considered other models with modified versions of the updating rules and still the same main results hold. For instance, instead of a sinusoidal time dependent probability of following either

the external signal or the weighted majority, we have tried a constant probability a. The dynamical rules are then modified to:

$$\mu_i(t+\tau) = \begin{cases} \text{sign}\left[\sum_{j\in V(i)} \omega_{ij}\mu_j(t)\right] & \text{w.p. } 1-a, \\ \text{sign}\left[\sin(\Omega t))\right] & \text{w.p. } a, \end{cases} \tag{4.18}$$

Another modification considers that the effect of the external influence is a factor to be considered simultaneously with the majority rule. In this case, the updating rule becomes:

$$\mu_i(t+\tau) = \text{sign}\left[\frac{1}{k_i}\sum_{j\in V(i)} \omega_{ij}\mu_j + asin(\Omega t)\right] \tag{4.19}$$

In both modified versions we have confirmed our main result, namely that there exists a value of the probability of repulsive links p for which the response adopts a maximum value.

We have discussed in some detail the microscopic mechanism for the amplification. We argued that the flexibility of the system to follow the external signal requires that the *local field* seen by each unit is kept close to zero and analysed how this condition might be achieved in some parameter limits.

A macroscopic analysis, in terms of a relaxation dynamics in a bistable potential, is able to explain the mean-field results. It is difficult to use this description beyond the mean field treatment, due to the presence of many metastable configurations. Because of their presence, a large response, corresponding to oscillations around (symmetrical) absolute minima can be obtained for a sufficiently slow forcing.

There are studies that point to the role network topology plays in synchronisation or response to stimuli [8]. Analysing the effect of coupling strength, degree distribution and other network characteristics on the coherent response may shed some light on how the mechanism can be optimised.

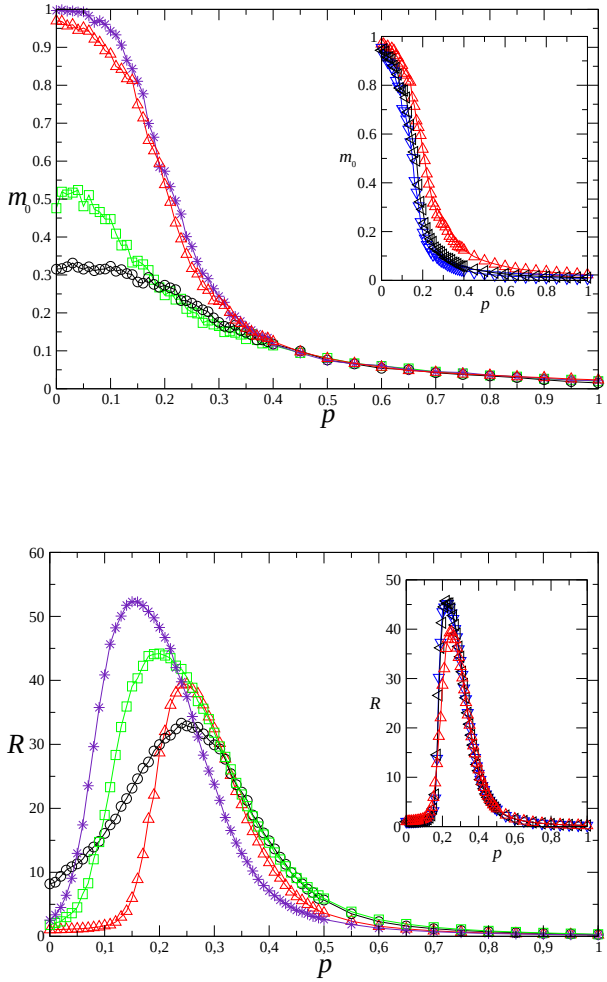

Figure 4.1: The coincidence between resonance and order-disorder transtion region. Upper panel: Modulus of the average magnetization as a function of the probability of repulsive links. In the regular networks, the existence of metaestable states reveals itself in a smaller magnetization at $p = 0$. Lower panel: Spectral amplification factor R versus probability of repulsive links p. Parameters are: $a = 0.15$, $\Omega = \frac{2\pi}{100}$, $\kappa = 1$. In the main graph, $N = 100$ and symbols correspond to topologies: ring with $k = 10$ neighbours ($\circ$), square lattice with $k = 8$ neighbours in the Moore neighbourhood ($\square$), and random networks with average number of neighbours $k = 10$ and rewiring probability $q = 0.2$ ($*$) and $q = 1$ ($\triangle$). In the inset, we chose the random network with $q = 1$, $k = 10$, and different curves correspond to sizes $N = 100$ ($\triangle$), 500 ($\triangleleft$), and 1000 ($\triangledown$).

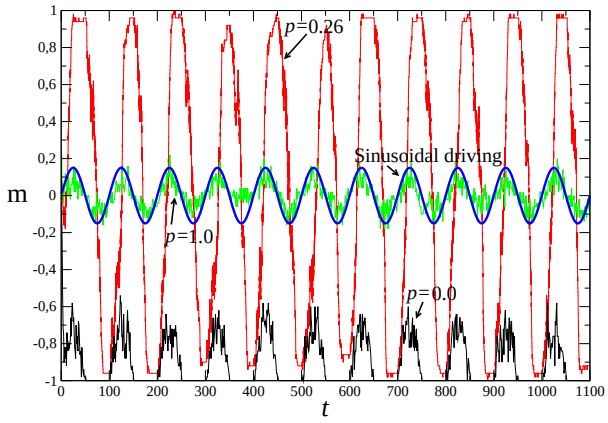

Figure 4.2: Evolution of magnetization in time (random network, $q = 1$, $k = 10$). Other parameters are: $N = 100$, $a = 0.15$, $\Omega = \frac{2\pi}{100}$, $\kappa = 1$.

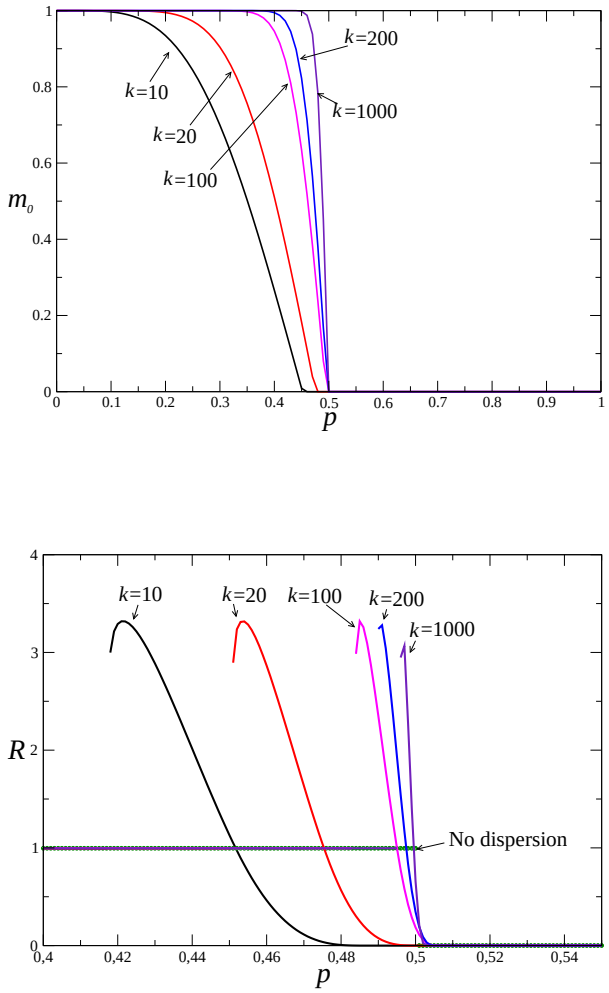

Figure 4.3: Upper panel: Modulus of the average magnetization as a function of the probability of repulsive links according to the mean-field theory for $\kappa = 1$. Lower panel: Spectral amplification factor versus probability of repulsive links according to the mean-field theory for $a = 0.15$, $\Omega = \frac{2\pi}{100}$, $\kappa = 1$.

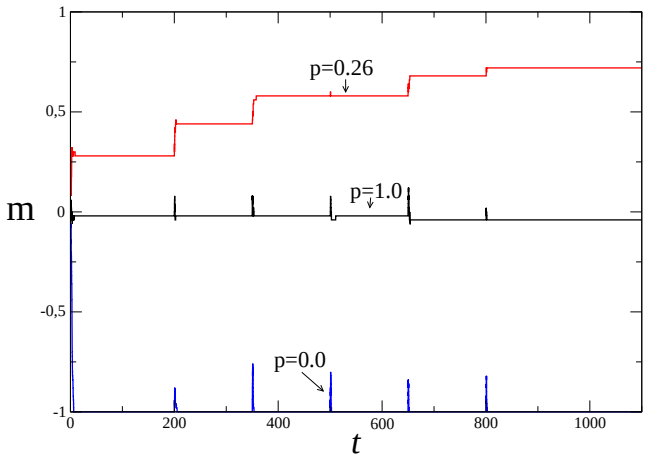

Figure 4.4: This image suggests that the step-by-step response we propose is a reasonable mechanism. Their outreach of the perturbations depends on the probability of repulsive links. At the optimal probability $p = 0.26$, the net effect of perturbations accumulates, but after the signal is switched off they don't continue spreading to the whole network.

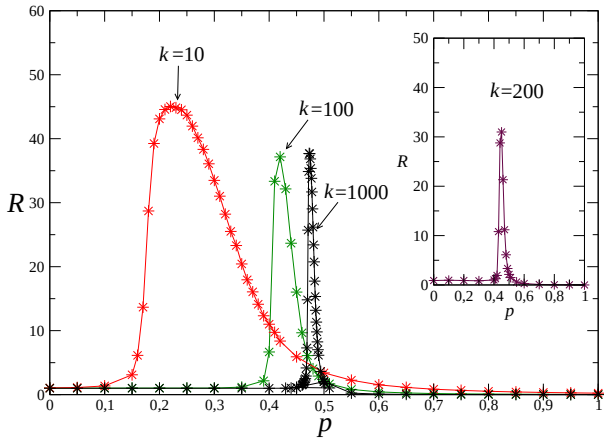

Figure 4.5: Spectral amplification factor versus probability of repulsive links for a random network with $q = 1$, $a = 0.15$, $\Omega = \frac{2\pi}{100}$, $\kappa = 1$. Main graph uses $N = 1001$ while the inset shows the case $N = 201$.

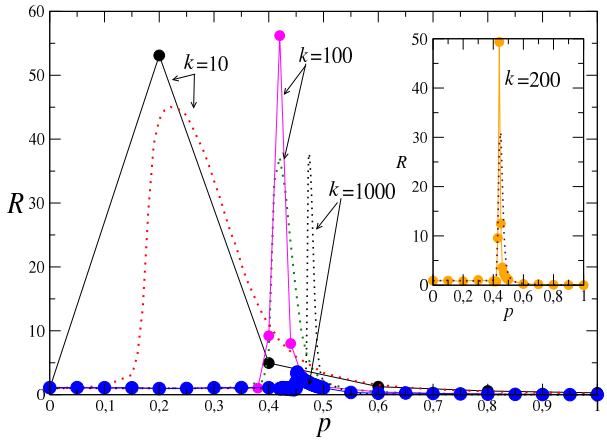

Figure 4.6: Spectral amplification factor versus probability of repulsive links for a "no-dispersion" network in which all sites have the same number of positive and negative links. Due to the particular way the network is constructed[41], only values of $p = k/N$ where the total number of neighbours per site, k, is an even integer number are allowed. Parameters are $N = 1001$, $a = 0.15$, $\Omega = \frac{2\pi}{100}$, $\kappa = 1$ (main graph) and $N = 201$ (inset). Note that the amplification region shrinks as k increases. For comparison, we also include as dotted lines the results of figure 4.5.

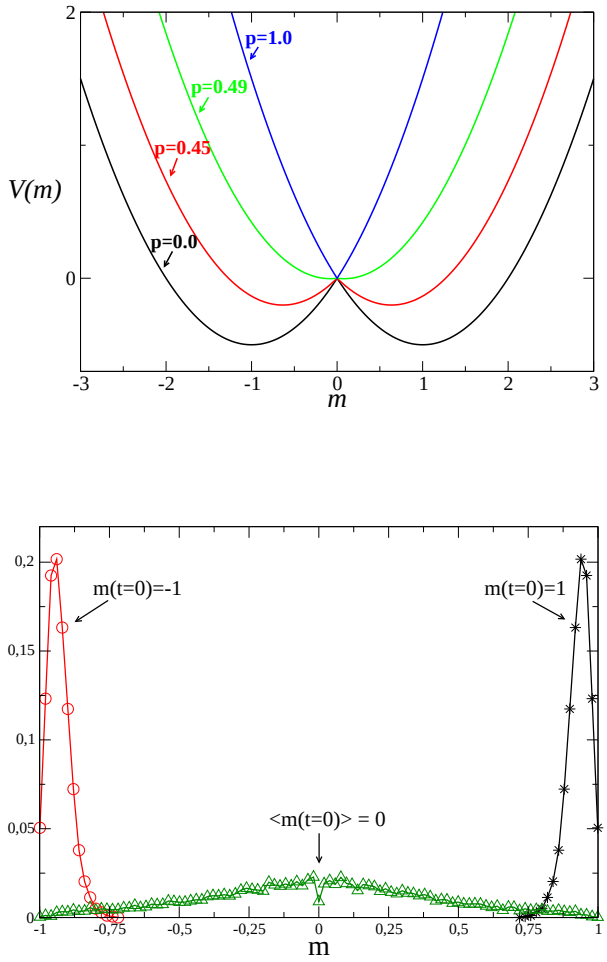

Figure 4.7: Comparison between the stable states predicted by mean field and simulations. Upper panel: the effective potential defining the relaxational dynamics according to Eq. 4.17, for different values of the probability of repulsive links p. We considered the case of $k = 100$. Lower panel: Distribution of stable states at the optimal probability $p_c = 0.25$ in the case of an unforced random network with $q = 1$, $N = 100$, $k = 10$, $\kappa = 1$ starting from three different initial conditions: all spins equal to $+1$ (data set indicated as $m(t = 0) = 1$), all spins equal to -1 ($m(t = 0) = -1$) and spins take randomly the value ± 1 ($\langle m(t = 0)\rangle = 0$).

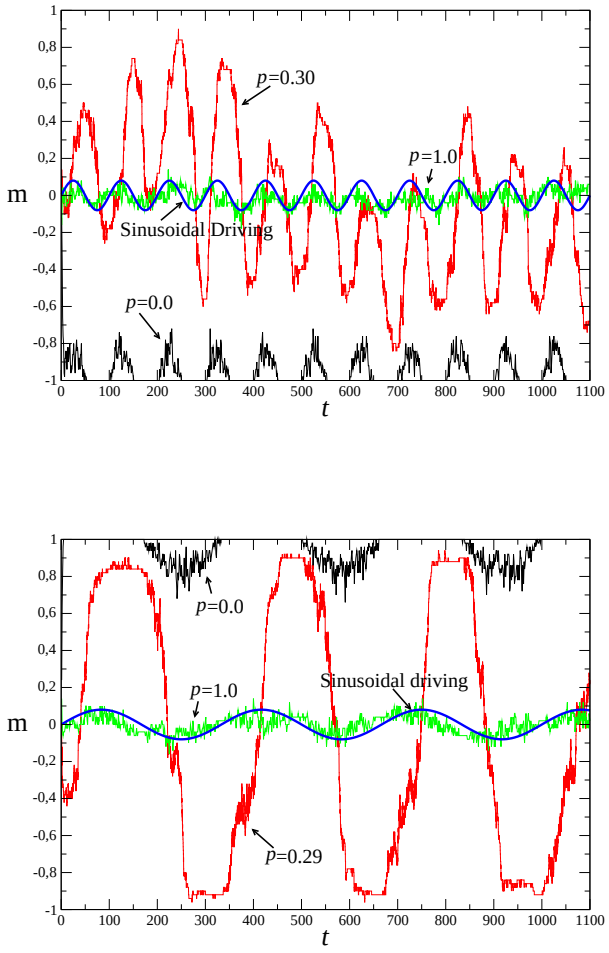

Figure 4.8: Upper panel: Evolution of the magnetization following a weak signal $a = 0.08$, $\Omega = \frac{2\pi}{100}$, in the case of a random network, $q = 1$, $k = 10$, $\kappa = 1$. The extreme values of the magnetization coincide with the points where the driving value changes sign, they don't take always the same value. This nonstationarity is explained by the influence of the random factors in our model. According to the proposed mechanism, the system walks in multi-steps (Fig. 4.4. The amplitude of the response depends on random factors, such as the sequence of perturbed nodes and their different local fields and connectivities. When the signal is weak and fast, these random factors influence the amplitude of the response, which explains the nonstationarity. Lower panel: Same as figure 4.8 for a slower forcing $\Omega = \frac{2\pi}{333.3}$. If is sufficiently slow, many nodes are perturbed, and at the end the system is able to display the maximum possible response and reach the points $m = \pm 1$.

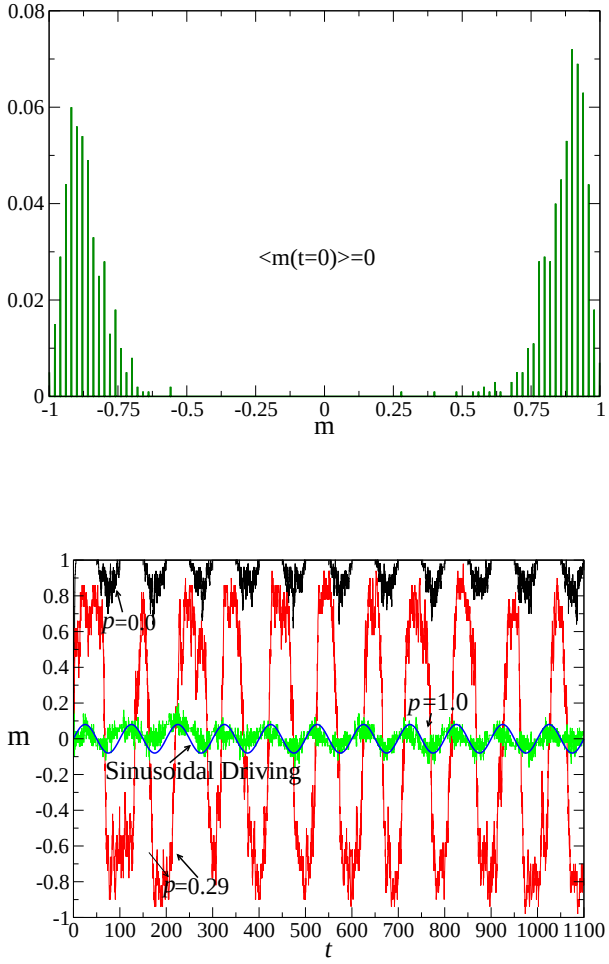

Figure 4.9: The influence of annealed disorder. Upper panel: Distribution of stable states at the optimal probability $p_c = 0.26$ in the case of an unforced random network with $q = 1$, $N = 100$, $k = 10$, $\kappa = 1$ starting from random initial conditions ($< m(t = 0) >= 0$). Lower panel: Evolution of the magnetization following a weak signal $a = 0.08$, $\Omega = \frac{2\pi}{100}$, in the case of a random network with annealed disorder in the interaction matrix, $q = 1$, $k = 10$, $\kappa = 1$.

Chapter 5

Conclusions, or what else could be done

We have shown that the presence of competitive interactions can optimize the response to weak signals, and gave as specific examples two models where the effect was verified. Furthermore, we unveiled the specific characteristics of this phenomenon, contrasting it to the case of disorder induced by noise or by diversity.

In our models, these three sources of disorder take advantage of different mechanisms to amplify the response: in the case of stochastic resonance, a time matching between switches induced by noise and the period of the signal, in the case of diversity induced resonance a lowering of the potential barrier between two stable states, and in the case of resonance induced by repulsive links the replacement of the bistable potential by a multistable one. Even though these later two are both instances of disorder induced resonance, so that both of them involve a lowering of barrier that renders weak signals supra-threshold, it is not clear how much they should be classified together. The kind of disorder we encountered was not predicted by the theory developed in [12], and far from being a minor detail, it has consequences in the type of response to very fast or very weak signals.

Future research should proceed along 3 directions. In the first place, more important than listing different sources of disorder, is to understand different mechanisms of resonance, that eventually can be exploited by any source of disorder, under appropriate circumstances.

Throughout the thesis, we reviewed a list of sources of disorder and compared its effects on two very generic models. Since both of those models are bistable systems, a second avenue of research would explore the boundaries of application of the phenomenon in other types of systems, such as excitable systems or oscillators. This is already underway: a system of nonlinear Van der Pol oscillators exhibits a similar phenomenon.

The third challenge is to find out whether the concepts developed in this thesis in an idealised manner would work in more realistic and complex circumstances. For instance, we adopted the language of sociophysics when we described the Ising-like model. It is a long standing debate whether such generic simple models actually have any interest in modeling social life. The *Divide and Conquer* maxim is well-known and widely applied for millennia, since the Romans, at least. It would be good to extract from the model what is specifically new, and to device a way to test it. We attempted a preliminary research of this topic, with the help of sociologists, but so far we have not been able to implement a completed project based on it.

Appendix A

Spectral Analysis

In this appendix I will give some details about the spectral analysis calculations used in Chapter 3.

A.0.1 What can the Laplacian represent?

Let's us consider a generic linearly coupled model, where $F(x_i)$ is any function of x_i:

$$\frac{dx_i}{dt} = F(x_i) + \frac{C}{N}\sum_{j=1}^{N} J_{ij}(x_j - x_i) \tag{A.1}$$

Defining the "Laplacian" [42] as $J'_{ij} = J_{ij} - \delta_{ij}\sum_{k=1}^{N} J_{kj}$, we rewrite Eq. A.1 as:

$$\frac{dx_i}{dt} = F(x_i) + \frac{C}{N}\sum_{j=1}^{N} J'_{ij}x_j \tag{A.2}$$

If Eq. A.1 models a potential system, $\frac{dx_i}{dt} = -\frac{\partial V}{\partial x_i}$, and the global potential is:

$$V(x_i, x_j, ...) == -\int F(x_i)dx_i dx_j + \frac{1}{4}\sum_{j}\sum_{i} J'_{ij}x_j x_i \tag{A.3}$$

We see $\sum_{i,j} J'_{ij} x_i x_j = -\sum_{i,j} J_{ij}(x_i - x_j)^2$ [42], because:

$$\sum_j \sum_i J'_{ij} x_i x_j = \sum_j \sum_i \left[J_{ij} - \delta_{ij} \sum_{k=1}^{N} J_{kj} \right] x_i x_j =$$
$$\sum_j \left[\sum_i J_{ij} x_j x_i \right] - \sum_j \left[\sum_i \left(\delta_{ij} \sum_{k=1}^{N} J_{kj} x_i x_j \right) \right] =$$
$$\sum_j \left[J_{1j} x_1 x_j + J_{2j} x_2 x_j + ... \right] - \sum_j \left[\sum_i \left(J_{1i} x_i^2 + J_{2i} x_i^2 + ... \right) \right] =$$
$$\left[J_{11} x_1^2 + J_{22} x_2^2 + ... + J_{12} x_1 x_2 + J_{21} x_2 x_1 + ... \right] - \sum_j \left(J_{11} x_1^2 + J_{12} x_1^2 + ... + J_{21} x_1^2 + J_{22} x_2^2 + ... \right) =$$
$$\left[J_{11} x_1^2 + J_{22} x_2^2 + ... + J_{12} x_1 x_2 + J_{21} x_2 x_1 + ... \right] - \left(J_{11} x_1^2 + J_{12} x_1^2 + ... + J_{21} x_1^2 + J_{22} x_2^2 + ... \right) =$$
$$\sum_j \sum_i J_{ij} x_j x_i - J_{11} x_1^2 - J_{22} x_2^2 - ... - J_{12} x_1^2 - ... - J_{21} x_1^2 - ... =$$
$$- \left[\sum_j \sum_i J_{ij} x_i^2 - \sum_j \sum_i J_{ij} x_i x_j \right] = -\frac{1}{2} \sum_j \sum_i J_{ij} (x_j - x_i)^2 \tag{A.4}$$

And so the global potential is:

$$V(x_i, x_j, ...) = -\int F(x_i, x_j, ...) dx_i dx_j ... - \frac{1}{4} \sum_j \sum_i J_{ij} (x_j - x_i)^2 \tag{A.5}$$

If the variables x_i represent some perturbation, we conclude [42] that in heuristic terms the positive eigenvalues of the Laplacian express the contribution of the coupling term to the vulnerability of the system to perturbations.

A.0.2 Spectral analysis

Let's us assume the state of a unit i is s_i^o at a given time. Our goal is to see how the interaction with the other units modifies this state.

We define the eigenvalues Q_α and (normalized) eigenvectors $e^\alpha = (e_1^\alpha, \ldots, e_N^\alpha)$ of the Laplacian coupling matrix J'_{ij}

$$J'_{ij} = J_{ij} - \delta_{ij} \sum_{k=1}^{N} J_{kj}, \tag{A.6}$$

$$\sum_{j=1}^{N} J'_{ij} e_j^{\alpha} = Q_{\alpha} e_i^{\alpha}. \tag{A.7}$$

with the normalization condition:

$$\sum_{i} e_i^{\alpha} e_i^{\beta} = \delta_{\alpha\beta} \tag{A.8}$$

The translation invariance of the system requires that:

$$\sum_{j=1}^{N} J'_{ij} = 0 \tag{A.9}$$

$$x_i = \sum_{\alpha=1}^{N} B_{\alpha} e_i^{\alpha}, \tag{A.10}$$

Now let's replace some terms in the equation 3.1 as:

$$\begin{aligned}
\sum_{j=1}^{N} J_{ij}(s_j - s_i) &= \sum_{j=1}^{N} J'_{ij} s_j && \text{(A.11)} \\
&= \sum_{j=1}^{N} J'_{ij}(s_j^o + x_j) && \text{(A.12)} \\
&= \sum_{j=1}^{N} J'_{ij} s_j^o + \sum_{j=1}^{N} J'_{ij} \sum_{\alpha=1}^{N} B_{\alpha} e_j^{\alpha} && \text{(A.13)} \\
&= \sum_{j=1}^{N} J'_{ij} s_j^o + \sum_{\alpha=1}^{N} B_{\alpha} Q_{\alpha} e_i^{\alpha} && \text{(A.14)}
\end{aligned}$$

$$\begin{aligned}
s_i &= s_i^o + x_i && \text{(A.15)} \\
&= s_i^o + \sum_{\alpha=1}^{N} B_{\alpha} e_i^{\alpha} && \text{(A.16)} \\
& && \text{(A.17)}
\end{aligned}$$

$$
\begin{aligned}
s_i^3 &= (s_i^o + x_i)^3 && \text{(A.18)}\\
&= ((s_i^o)^2 + x_i^2 + 2s_i^o x_i)(s_i^o + x_i) && \text{(A.19)}\\
&= (s_i^o)^3 + (s_i^o)^2 x_i + s_i^o x_i^2 + x_i^3 + 2(s_i^o)^2 x_i + 2s_i^o x_i^2 && \text{(A.20)}\\
&= (s_i^o)^3 + 3(s_i^o)^2 x_i + 3s_i^o x_i^2 + x_i^3 && \text{(A.21)}
\end{aligned}
$$

$$
s_i - s_i^3 = s_i^o + x_i - (s_i^o)^3 - 3(s_i^o)^2 x_i - 3s_i^o x_i^2 - x_i^3 \qquad \text{(A.22)}
$$

Expanding the right side of Eq.(3.1) for $A = 0$, multiplying the resulting equation by e_i^α, and considering the normalization condition A.8, we get:

$$
\begin{aligned}
&(s_i^o)e_i^\alpha + x_i e_i^\alpha - (s_i^o)^3 e_i^\alpha 3(s_i^o)^2 x_i e_i^\alpha - 3s_i^o x_i^2 e_i^\alpha - x_i^3 e_i^\alpha = \\
&= (s_i^o)e_i^\alpha + \sum_{\beta=1}^{N} B_\beta e_i^\beta e_i^\alpha - (s_i^o)^3 e_i^\alpha - 3(s_i^o)^2 \sum_{\beta=1}^{N} B_\beta e_i^\beta e_i^\alpha - 3s_i^o \left[\sum_{\beta=1}^{N} B_\beta e_i^\beta\right]^2 e_i^\alpha - \left[\sum_{\beta=1}^{N} B_\beta e_i^\beta\right]^3 e_i^\alpha = \\
&= (s_i^o)e_i^\alpha + \sum_{\beta=1}^{N} B_\beta e_i^\beta e_i^\alpha - (s_i^o)^3 e_i^\alpha - 3(s_i^o)^2 \sum_{\beta=1}^{N} B_\beta e_i^\beta e_i^\alpha - 3s_i^o \sum_{\beta,\gamma=1}^{N} B_\beta B_\gamma e_i^\beta e_i^\gamma e_i^\alpha - \\
&- \sum_{\beta,\gamma,\eta=1}^{N} B_\beta B_\gamma B_\eta e_i^\beta e_i^\gamma e_i^\eta e_i^\alpha
\end{aligned}
$$

We will assume that:

$$
\frac{1}{N}\sum_{i=1}^{N} s_i^o e_i^\alpha \approx \frac{1}{N^2}\sum_{i=1}^{N} s_i^o \sum_{i=1}^{N} e_i^\alpha \qquad \text{(A.23)}
$$

Which is true in the limit of $N \to \infty$

Also:

$$
\sum_{i=1}^{N} e_i^\alpha = 0 \qquad \text{(A.24)}
$$

unless $Q_\alpha = 0$

Now let's average over all elements, to find the evolution of a given mode.

$$\frac{dB_\alpha}{dt} = -\sum_{\beta,\gamma,\eta} F^{\beta\gamma\eta\alpha} B_\beta B_\gamma B_\eta + \left(C\frac{Q_\alpha}{N} - K \right) B_\alpha, \tag{A.25}$$

where

$$F^{\beta\gamma\eta\alpha} = \sum_{i=1}^{N} e_i^\beta e_i^\gamma e_i^\eta e_i^\alpha, \tag{A.26}$$

$$K = \frac{3}{N}\sum_{i=1}^{N} (s_i^o)^2 - 1. \tag{A.27}$$

If we neglect the coupling between modes, this approximation leads to $F^{\beta\gamma\eta\alpha} = 1/\mathrm{PR}_\alpha$ if $\alpha = \beta = \gamma = \eta$ and 0 otherwise. We then obtain the following equation for the amplitude of the α-th mode:

$$\frac{dB_\alpha}{dt} = -B_\alpha^3 + \mathrm{PR}_\alpha \left(C\frac{Q_\alpha}{N} - K \right) B_\alpha. \tag{A.28}$$

According to this approximation, unless $Q_\alpha > \frac{KN}{C}$, the amplitude of the mode B_α tends to zero, and any small perturbation vanishes. Otherwise, the amplitude of the mode α tends to a steady state value:

$$B_\alpha = \pm \left[\sqrt{\mathrm{PR}_\alpha \left(C\frac{Q_\alpha}{N} - K \right)} \right]. \tag{A.29}$$

In this case, mode α is said to be an *open mode*.

Appendix B

A method to detect potential wells

In this appendix, I explain how we detected the number of states, by adapting the method poposed in V. N. Livina, F. Kwasniok, and T. M. Lenton, Clim. Past, 6, 77-82, (2010)

The method was developed to detect the number of states in geophysical time series, which are have observational noise and often nonstationarities. Therefore, the method [58] starts considering a stochastic Langevin equation:

$$\dot{z} = -U'(z) + \sigma\eta, \tag{B.1}$$

where $U(z)$ is a potential function, σ is the noise level and η is a Gaussian white noise with zero mean and unit variance. In the context of the original work, the state variable z represents some large-scale climate variable like temperature.

We assume a general polynomial potential:

$$U(z) = \sum_{i=1}^{L} a_i z^i, \tag{B.2}$$

where the order L is even and the leading coefficient a_L is positive for eq. (B.1) to possess a stationary solution. The order of the polynomial controls the complexity of the potential (the number of potential wells), with increasing values

of L allowing more states to be accommodated: a fourth-order polynomial can capture a system with two states (double-well potential).

The number of system states is estimated by means of a polynomial fit of the probability density function of the data. Suppose the system is governed by eq. (B.1). The corresponding Fokker-Planck equation for the probability density function $p(z,t)$

$$\partial_t p(z,t) = \partial_z[U'(z)p(z,t)] + \frac{1}{2}\sigma^2\partial_z^2 p(z,t) \tag{B.3}$$

has a stationary solution given by (see [18])

$$p(z) \sim \exp[-2U(z)/\sigma^2]. \tag{B.4}$$

Given this one-to-one correspondence between the potential and the stationary probability density of the system, the potential can be reconstructed from time series data of the system as

$$U = -\frac{\sigma^2}{2}\log p_{\mathrm{d}}, \tag{B.5}$$

where p_{d} is the empirical probability density of the data. This is estimated using a standard Gaussian kernel estimator [53]. Then least-square fits of $-\log p_{\mathrm{d}}$ (weighted with the probability density of the data with polynomials of increasing even order L are calculated, starting with $L = 2$, until a negative leading coefficient a_L is encountered. The polynomial of highest degree before first obtaining a negative leading coefficient is considered the most appropriate representation of the probability density of the time series, both locally and globally, avoiding overfitting of sampling fluctuations in the probability density.

The number of states S in the system is then determined as

$$S = 1 + \frac{I}{2}, \tag{B.6}$$

where I is the number of inflection points of the fitted polynomial potential of appropriate degree L as described above. This definition takes into account not only the degree of the polynomial but its actual shape. We only look at even-order potentials with positive leading coefficient. These have positive curvature both at minus and plus infinity. Thus, inflection points can only occur in pairs (if any). Any potential has at least one state (with no inflection points). Then

we count one further state for each pair of inflection points. This can be either a real minimum (well) or just a flattening in the potential (corresponding to degeneracies in the potential; definition (B.6) accommodates both possibilities. The number of inflection points is numerically given as the number of sign changes in the second derivative on a fine enough mesh.

If necessary, the coefficients that determine the shape of the potential are then estimated using the unscented Kalman filter (UKF). The method was developed for the stochastic model with noise component and performs polynomial fit of the histogram which is expected to be smooth (i.e. no discrete peak). To detect the number of states in the ϕ^4 model with competitive interactions, we had to add a noise component to the model trajectories to make the method applicable. Yet, to minimise the effect of noise, we considered white Gaussian noise of small amplitude (0.01 of the trajectory amplitude), which allowed us to "fill" the histogram and make it suitable for smooth polynomial fit. Note that adding noise can only hide a certain shallow well in the potential, but never lead to a false detection of non-existent states, and therefore adding noise cannot lead to false detection of additional states.

Appendix C

The rewiring algorithm mentioned in the Divide and Conquer chapter

To settle the issue of whether the resonance phenomenon was induced by variability in the number of repulsive links or not, we decided to construct a network in which every agent had exactly the same number of positive and of repulsive links. We did so, adapting the "local rewiring algorithm" (S. Maslov, K. Sneppen, Science **296**, 910 (2002)) to construct a random network where every node has exactly the same number of links k and the same proportion p of repulsive links – the "no dispersion" network.

In a network with N nodes each with $2k$ neighbours, there will be $2pk$ repulsive links.

The network is constructed as follows: we start with a ring where each of the N nodes has $2k$ nearest neighbours. Then we randomize the network by repeating the elementary rewiring step: we select two links at random, and rewire them by switching partners, excluding the appearance of multiple edges. If we want a global coupled network, the randomised links will be all repulsive, and we later

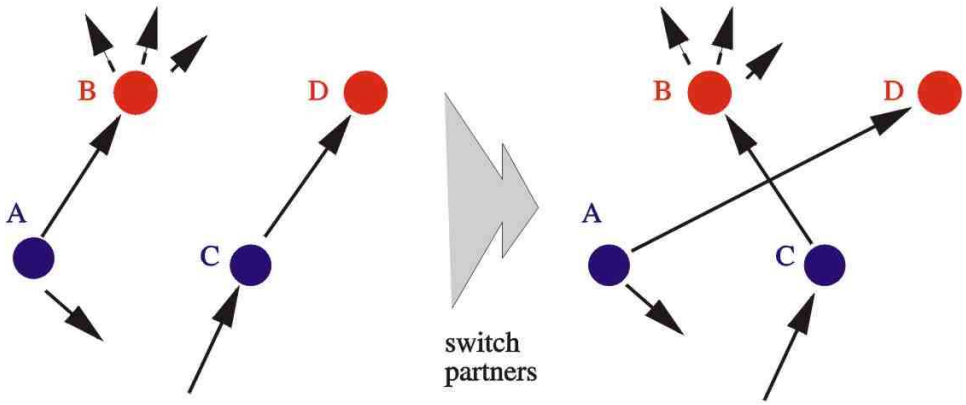

Figure C.1: An illustration of the rewiring algorithm. A pair of directed edges A – ¿ B and C – ¿ D is randomly selected. These edges are then rewired in such a way that A becomes connected to D, while C to B, provided that none of these edges already exist in the network, in which case the rewiring step is aborted and a new pair of edges is selected. The rewiring algorithm conserves both the in- and out-connectivity of each individual node. Source: http://www.cmth.bnl.gov/ maslov/

add attractive links until everyone is coupled. Otherwise, the first *2pk* links in the ring to be randomised are repulsive, and the rest *(1-p)2k* are attractive.

Appendix D

Publications

The publications concerning the results in this thesis are:

D.0.2.1 ϕ^4 model

T. Vaz Martins, V. N. Livina, A. P. Majtey, R. Toral, Resonance induced by repulsive interactions in a model of globally-coupled bistable systems, Physical Review E **81**, 041103 (2010)

D.0.2.2 Opinion formation model

- T. Vaz Martins and Raúl Toral, Resonance induced by repulsive links, in *Applications of Nonlinear Dynamics: Model and Design of Complex Systems*, edited by V. In, P. Longhini, A. Palacios, (Springer Verlag, 2009), p. 439
- T. Vaz Martins, R. Toral, M.A. Santos, Divide and Conquer: Resonance Induced by Competitive Interactions, European Physical Journal B **67**, 329-336 (2009)

———————-

References

[1] E. W. Jacobs A. R. Bulsara A. D. Hibbs, A. L. Singsaas and J. J. Bekkedahl. *J. Appl. Phys.*, **77**:2582, 1995. 7

[2] L. A. Pérez A. Radillo-Díaz and M. Del Castillo-Mussot. *Phys. Rev. E*, **80**:066107, 2009. 37

[3] P. W. Anderson. *Phys. Rev.*, **109**:1492, 1958. 26

[4] P. W. Anderson. *Mater. Res. Bull.*, **5**:549, 1970. 26

[5] R. Axelrod. *J. Conflict Res.*, **41**:203, 1997. 36

[6] K. Wiesenfeld B. McNamara and R. Roy. *Phys. Rev. Lett.*, **60**:2626, 1988. 6, 7

[7] P. Babinec. *Physics Letters A*, **225**:179, 1997. 34

[8] Y. Bar-Yam and I. R. Epstein. *PNAS*, **101**:4341, 2004. 48

[9] R. Benzi. Stochastic resonance: from climate to biology. **eprint arXiv:nlin/0702008**, 2007. 6

[10] P. Bourdieu. *La distinction: critique sociale du jugement*. Les editions de minuit edition, 1979. 36

[11] S. Fortunato C. Castellano and V. Loreto. *Rev. Mod. Phys.*, **81**:591, 2009. 33

[12] R. Toral C. Tessone, C.R. Mirasso and J.D. Gunton. *Phys. Rev. Lett.*, **97**:194101, 2006. i, ii, 7, 8, 14, 18, 31, 45, 57

[13] D.H. Zanette C.J. Tessone and R. Toral. *Eur. Phys. J. B*, **62**:319, 2008. 16, 31, 32, 42

[14] Desai and Zwanzig. *J. Stat. Phys*, **19**:1, 1978. 9

[15] ed. A. P. Young. *Spin glasses and random fields*. World Scientific, Singapore, 1997. 18, 19

[16] F. Amblard G. Deffuant, D. Neau and Weisbuch G. *Advances in Complex Systems*, **3**:87, 2000. 33

[17] Andrey Ganopolski and Stefan Rahmstorf. *Phys. Rev. Lett.*, **88**:038501, 2002. 6

[18] C. W. Gardiner. *Handbook of Stochastic Methods for Physics, Chemistry and the Natural Sciences*. Springer-Verlag, Berlin, third edition edition, 2004. 65

[19] A. Giddens. *Sociology*. (5th edition) polity, cambridge edition, 2006. 36

[20] J. Zhang H. Cheng and J. Liu. *Phys. Rev. E*, **75**:041910, 2007. 14

[21] P. Hänggi and F. Marchesoni. Topical issue on stochastic resonance. i, 3

[22] R. Hegselmann and U. Krause. *Journal of Artificial Societies and Social Simulation (JASSS*, **5**:2, 2002. 33

[23] J. A. Almendral I. Leyva, I. Sendiña-Nadal and M. A. Sanjun. *Phys. Rev. E*, **74**:056112, 2006. 16, 32, 33, 37

[24] V.M. Eguluz J. C. Gonzlez-Avella, M.G. Cosenza and M. San Miguel. *New Journal of Physics*, **12**:013010, 2010. 34

[25] W. L. Ditto M. E. Inchiosa J. F. Lindner, B. K. Meadows and A. Bulsara. *Phys. Rev. Lett.*, **75**:3, 1995. 13

[26] Carson C. Chow J. J. Collins and Thomas T. Imhoff. *Phys. Rev. E*, **52**(4):R3321, 1995. 7

[27] S.Lozano J.A. Acebrón and A. Arenas. *Phys. Rev. Lett.*, **99**:128701, 2007. 14

[28] E. Pantazelou J.K. Douglass, L. Wilkens and F. Moss. *Nature*, **365**:337, 1993. 7

[29] Meghan E. Wills Adi R. Bulsara John F. Lindner, Barbara J. Breen and William L. Ditto. *Phys. Rev. E*, **63**:051107, 2001. 7

[30] P. Jung and P. Hänggi. *Europhys. Lett.*, **8**:505, 1989. 6, 11, 18, 38

[31] H. A. Kramers. *Physica*, **7**:284, 1940. i, 3, 5

[32] M. Kuperman and D. Zanette. *Eur. Phys. J. B*, **26**:387, 2002. 33, 34, 35, 36, 37, 47

[33] E. Menichella-Saetta L. Gammaitoni, F. Marchesoni and S. Santucci. *Phys. Rev. Lett.*, **62**:349, 1989. 6

[34] P. Jung L. Gammaitoni, P. Hänggi and F. Marchesoni. *Rev. Mod. Phys.*, **70**:223, 1998. i, 3, 7, 31

[35] D.P. Landau and K. Binder. *A Guide to Monte Carlo Simulations in Statistical Physics*. Cambridge university press edition, 2000. 38

[36] André Longtin and Dante R. Chialvo. *Phys. Rev. Lett.*, **81**:4012, 1998. 7

[37] J. Lorenz. *Int. J. Mod. Phys. C*, **18**:1819, 2007. 33

[38] E. Glatt M. Gassel and F. Kaiser. *Phys. Rev. E*, **76**:016203, 2007. 14

[39] M. Gosak M. Perc and S. Kralj. *Soft Matter*, **4**:1861, 2008. 14, 27

[40] R. Toral M. Pineda and E. Hernandez-Garcia. *Journal of Statistical Mechanics: Theory and Experiment*, **P08001**:1, 2009. 35

[41] S. Maslov and K. Sneppen. *Science*, **296**:910, 2002. ix, 44, 53

[42] P. N. McGraw and M. Menzinger. *Phys. Rev. E*, **77**:031102, 2008. 17, 27, 32, 59, 60

[43] B. McNamara and K. Wiesenfeld. *Phys. Rev. A*, **39**:4854, 1989. 5

[44] M. San Miguel and R. Toral. *Stochastic effects in physical systems, in* Instabilities and Nonequilibrium Structures VI. Kluwer Academic Publishers, 35-130, eds. e. tirapegui, j. martńez and r. tiemann edition, 2000. 18

[45] C. Nicolis and G. Nicolis. *Tellus*, **33**:225, 1981. 3, 5

[46] L. Ward P. Greenwood and W. Wefelmeyer. *Phys. Rev. E*, **60**:4687, 1999. 6

[47] A. Sutera R. Benzi and A. Vulpiani. *J. Phys. A*, **14**:453, 1981. 3, 5

[48] C. J. Tessone R. Toral and J. Viana Lopes. *Eur. Phys. J. Special Topics*, **143**:59, 2007. i, vi, 7, 12, 13

[49] E. Hernandez-Garcia R. Toral and J. D. Gunton. *International Journal of Bifurcation and Chaos*, **19, 10**:3499, 2009. 14

[50] G. Deffuant G. S. Huet and W. Jager. *Advances in Complex Systems*, **11,4**:529, 2008. 37

[51] L. Salzarulo. *Journal of Artificial Societies and Social Simulation*, **9(1)**:13, 2006. 37

[52] Y. Shinomoto and Y. Kuramoto. *Prog. Theor. Phys.*, **75**:1105, 1986. 16

[53] Silverman. *Density estimation for statistics and data analysis.* Chapman and hall edition, 1986. 65

[54] K. Sznajd-Weron and J. Sznajd. *Int. J. Mod. Phys. C*, **11**:1157, 2000. 33

[55] A. Sato T. Munakata and T. Hada. *J. Phys. Soc. Japan*, **74**:2094, 2005. 6

[56] R. Toral T. Vaz Martins and M.A. Santos. *Eur. Phys. J. B*, **67, N. 3**:329, 2009. ii, 26

[57] C. J. Tessone and R. Toral. *Eur. Phys. J. B*, **71**:549, 2009. ii, 34, 35

[58] F. Kwasniok V. N. Livina and T. M. Lenton. *Clim. Past Discuss.*, **5**:2223, 2009. 23, 64

[59] Jager W. and Amblard F. *Computational and Mathematical Organization Theory*, **10**:295, 2004. 37

[60] D. J. Watts and S. H. Strogatz. *Nature*, **393**:440, 1998. 37

[61] H.S. Wio. *Phys. Rev. E*, **54**:R3075, 1996. 14